Non-Destructive Material Defect Analysis of Metals and Composites via Thermography

James Chapman

Jonathan Doubt

California Polytechnic State University, San Luis Obispo

Department of Materials Engineering

Table of Contents

Contents

List of Figures

Non-Destructive Material Defect Analysis of Metals and Composites via Thermography

James Chapman*, Jonathan Doubt*

**Students at California Polytechnic State University, San Luis Obispo, Department of Materials Engineering*

Abstract

The Naval Surface Warfare Center, Port Hueneme Division, is interested in the development of non-destructive damage assessment of shipboard materials via drones at distance. Long Pulsed Thermography (LPT), a method of non-destructive evaluation, was investigated as a possible method for detecting damage in metals (5005h24 Al alloy and 1008 carbon steel) and composites (aramid fiber honeycomb sandwich structure) at distances from 0.5 m to 3.0 m. LPT was conducted using two 1000 W can lights to heat the samples, and a FLIR E8-XT thermal camera. The images were then analyzed using ImageJ software to determine if damage could be detected from the thermal images. LPT detected damage most consistently in the composite material at distances of 0.5 m and 1.5 m. Camera resolution limited measurement at longer distances. Damage was only detectable at 0.5 m in both metal samples due to the reflection of heat from their surfaces. Though the ImageJ software was able to detect some defects that were visually detectable in the thermal images, it failed to consistently or accurately determine damage size. This study shows that damage detection is possible at near distances (0.5 m-1.5 m) for composites and even shorter distances for metals. However, characterization of samples with marine coatings aided by better image analysis algorithms are needed prior to implementation of this technology.

1. Literature Review

1.1. Introduction

The U.S. Navy faces a serious problem when assessing the material defects within various components within their ships. If left undetected these defects can cause serious damage to the vessels and will affect the overall preparedness of the Navy. Getting to certain locations on top of ships can be hazardous to people. So, the Navy is searching for ways to remotely detect damage. This paper will investigate ways to detect material defects that can be implemented onto a drone for remote detection.

1.2. Background

For this project, any method used to detect damage must be non-destructive to the material and must be able to scan the material without touching it. The method must be non-destructive so the material can continue being used if no defects are found. Being able to scan from a distance will be useful when implementing the equipment onto the drones for remote detection. One method that is both non-destructive and can be used at a distance is infrared thermography.

Infrared thermography, also known as IR thermography, is a process in which the sample that is being imaged is heated up, then using an infrared camera, an image of the sample is captured showing the infrared radiation being emitted from the heated sample. This image is produced by the infrared camera by taking the infrared waves that are emitted and turning it into an image that can be used to analyze the sample. Figure 1 shows how an IR camera works.

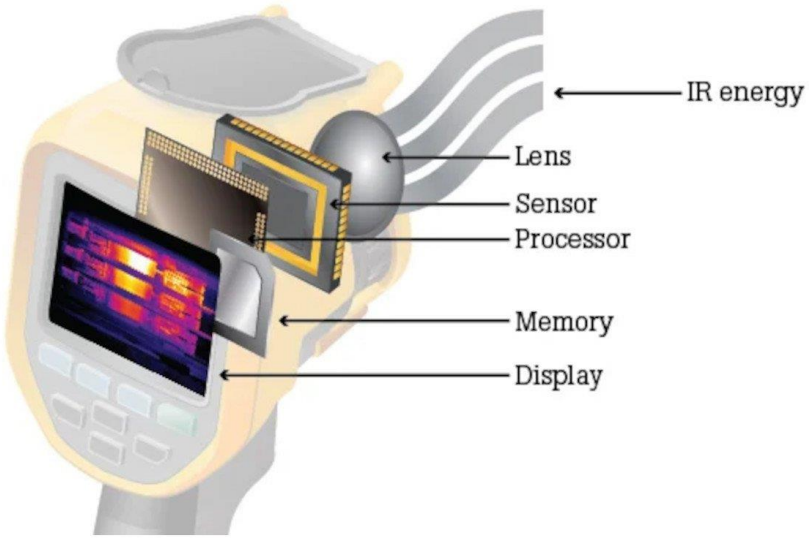

Figure 1: Diagram showing how a typical infrared camera works.

The main advantage of using IR thermography is its non-destructive testing ability, meaning the sample can be inspected without taking it out of service or needing a replacement [1]. This is ideal for naval ships because of the size of the shipboard panels that need to be inspected. It is very expensive and time-consuming to remove a shipboard panel, so nondestructive testing is advantageous to this process. The specific model being used for testing is the Teledyne FLIR E8-XT, shown in Figure 2.

Figure 2: Teledyne FLIR E8-XT infrared camera used for testing.

A type of IR thermography commonly used is directional thermography which involves heating one surface of the material using a uniform heat source at a distance, and then imaging the sample using an IR camera. The idea behind this heating is if no defects are present in the sample the heat will travel evenly through the sample and then return to the surface evenly. In the locations with defects present, the material will heat differently. This heating is typically accomplished by using high-powered lights as the heat source. If a very high-intensity light (>5 kW) is used to heat the sample the method is known as pulse or flash thermography [2]. In this method, the light is only active for a few milliseconds [1]. Another type of directional thermography is called long pulse thermography which uses lower intensity lights (500 W-1000 W) for a longer time to heat the sample, and then images are collected as the test cools down [3].

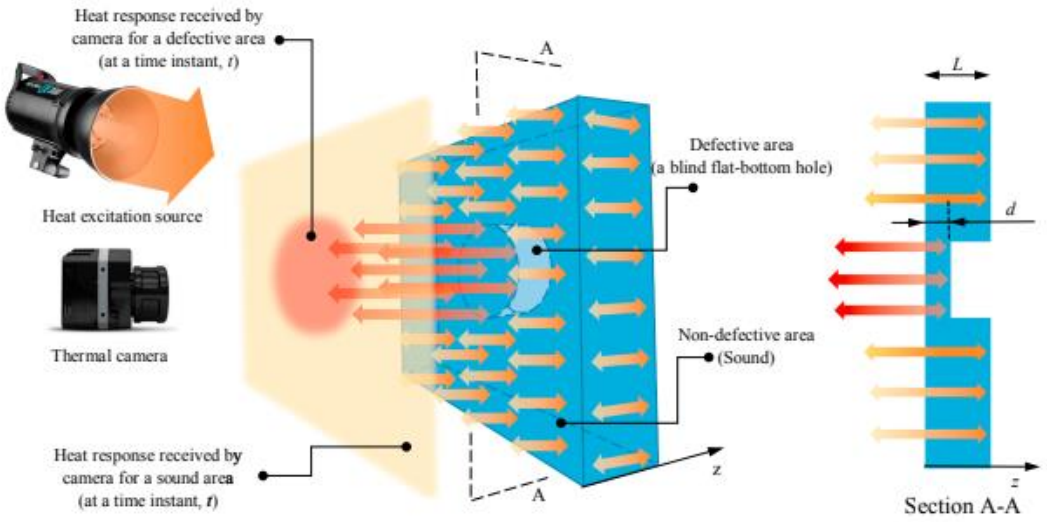

Figure 3:The heat diffusing through a sample with a defect present [1].

The advantage of pulse thermography is that it is a very fast test. The downside is that the equipment for this experiment is expensive, and because of the fast test it may not heat the material enough to expose deep defects. Long pulse thermography takes longer to run the tests but uses much less expensive equipment and sufficient more time can be given to heat the sample throughout [2]. Both methods are used frequently to test for defects in materials.

IR thermography has been used to detect defects in metals. Common types of metals used on naval ships are aluminum 5005h24 and 1008 carbon steel.

Aluminum 5005h24 is an aluminum magnesium alloy that cannot be heat treated. It is commonly used in alkaline marine conditions due to its corrosion resistance. Aluminum is a relatively soft metal. Throughout the material's service life, it is likely to get scratched or damaged due to its relative inability to resist surface wear.

Carbon steel is a type of steel alloy that contains up to 1.0 percent carbon and up to 1.65 percent manganese. 1008 carbon steel is a type of low carbon steel containing .06 percent carbon, .38 percent manganese, and .01 percent silicon, with additional trace elements and the remaining composition being iron. This makes the material stronger, but steel also oxidizes when exposed to oxygen for too long, and moisture accelerates the oxidation process [4]. Oxidation of metals is a form of corrosion that results in oxides building on the surface of the material which can cause the material to be weakened. Corrosion is an electrochemical reaction between the surface of a material and the environment it is in [5]. Carbon steel is not corrosion resistant like aluminum because of its chemically inert aluminum oxide layer that forms on the surface of the aluminum. Iron oxide (rust) is not inert and can spread beyond the surface of the steel and cause the sample to have weakened properties because of the oxidation. Due to the metal being used on naval vessels it is safe to assume that the carbon steel will be exposed to moisture.

IR thermography has been used to detect corrosion on and below the surface of metals. For carbon steel, IR thermography was able to detect blisters formed by corrosion on the surface of the material [6]. Thermography has also been used to detect surface defects on metals. Most of the experiments using IR thermography are conducted with the heat source between 10 cm and 40 cm from the sample.

Other materials commonly used in a naval vessel are honeycomb composites. Within composite materials, several material defects can form. These defects could be introduced to the composite during its creation or through general wear. One of the main types of defects found in these composites is delamination. Delamination is a separation between two layers of the composite that can be caused by shear and tensile forces that separate layers. In a honeycomb composite, this often occurs between the epoxy face and the core material. It results in a slightly bubbled look and can lead to sample failure [7]. IR Thermography has been used on honeycomb composites to detect defects; however, this method has primarily been tested at distances between 10 cm and 40 cm, like with the metal samples.

To detect any type or amount of damage in any of the materials the thermal camera must be able to detect a change in the temperature. The Teledyne FLIR E8-XT infrared camera used in this experiment has a thermal sensitivity of .05 °C [8]. This means for the camera to detect any change in temperature within the sample the face of the sample must be heated at least .05 °C. In this experiment, long pulse thermography will be used to supply the heat to the surface of the sample to raise the temperature. Heating the sample well above the minimum temperature will increase the likelihood that defects within the material will be visible. During the experiment, the samples should have a thermal gradient between the front and the back of the sample of at least 1.0 °C, and the back of the sample should be heated at least 1.0 °C above the room temperature. To find the amount of time needed to heat the samples at each distance, optimization testing is needed.

The long pulse thermography will be achieved with two halogen 1000 W narrow-angle bulbs. This method has been used before to detect defects within materials. In previous tests, it was IR thermography at around 50 cm from the samples [2, 3, 9]. Considering this, it is possible to determine the amount of power being delivered to the sample at any distance.

Defects in composites and metals have been detected in other experiments using long pulse thermography. In a study by Darryl Almond et. al, a CFRP sample with a thickness of 10 mm holes of varying depths and diameter were drilled which would be representative of in-plane defects which are like delamination. Two heating lamps were used with 1000 W bulbs at a distance of 0.4 m from the sample. After 5 s of heating, they were able to detect all material defects [3].

Another experiment was conducted using long pulse thermography by Zijun Wang et. al. They tested a composite with a thickness of 7.3 mm with holes drilled to various depths, and they had their heating lamps 0.3 m away from the sample. The long pulse thermography lasted 7 s and they were only able to detect 3 of the 8 holes drilled into the sample with just the raw images. Using post-image processing they were able to detect the other defects [2].

Post image processing should be considered for this experiment. It has the potential to increase the speed at which thermal images can be detected, which would be valuable. ImageJ is free image processing software and can be paired with thermal images to detect defects present in the images. This software will be used to identify and quantify the amount of the sample that contains a defect.

For this experiment longer distances than those previously researched will be tested. Keeping this in mind, this experiment will attempt to detect any defects in the samples from further distances.

1.3. Research Question

Taking into consideration the metals and composites, their defects, and the methods discussed to detect the defects, some questions arise. The primary question being: Using long pulse thermography at distances between 0.5 m and 3.0 m, is it possible to detect any of the following defects for the following materials?

- Aluminum 5005h24: surface wear
- 1008 Carbon Steel: oxidation and surface wear
- Aramid Fiber Honeycomb Sandwich Structure Composite: delamination

2. Methodology

2.1. Design of Experiment

For each of the materials three different samples were tested. The control parameters for this experiment were time and distance. To ensure accuracy in this experiment, each of the samples were tested at three distances. With 7 material samples, each tested 3 times at 3 distances, 63 total tests were taken. Due to the large difference in the three distances, block testing was used to reduce the possibility for error in varying distances often.

2.2. Materials

Three different materials were tested in this experiment, a composite sample, an aluminum sample, and a steel sample. All samples were obtained from the Office of Technology at the Naval Surface Warfare Center, Port Hueneme Division.

The aluminum samples were 5005h24 aluminum alloy. This is an aluminum magnesium alloy. The sample has a thickness of 0.0863 cm. Scratches were introduced to this sample using 60 grit sandpaper wrapped over the tip of a pen. The two scratches were along the diagonals of the face of the sample. This damage was introduced to determine if small surface imperfections can be detected using the long pulse thermography method.

The steel samples were 1008 carbon steel. They had a thickness of 0.0812 cm. Samples of the steel were placed outside for a period of 3 months located approximately 1000 feet from the shoreline. This was done to oxidize the steel so the long pulse thermography's ability to detect rust on steel surfaces could be tested.

The composite was made of a honeycomb core with an epoxy face and back. The core was made of an unknown material. Based on its appearance the material is likely aramid fiber. The core material had a thickness of 1.192 cm. The epoxy face and back had thicknesses of 0.114 cm. This brought the total thickness of the material to 1.424 cm. Voids and defects were introduced into the composite so the long pulse thermography method can be tested for the material.

2.3. Set up

Two 1000 W Sylvania 56206 bulbs are used as the heat source for this experiment. The thermal camera used in the experiment was a Teledyne FLIR E8-TX. Figure 4 shows how the experiment was set up. To ensure that the lights did not draw too much power from a single outlet each light was plugged into a separate wall outlet.

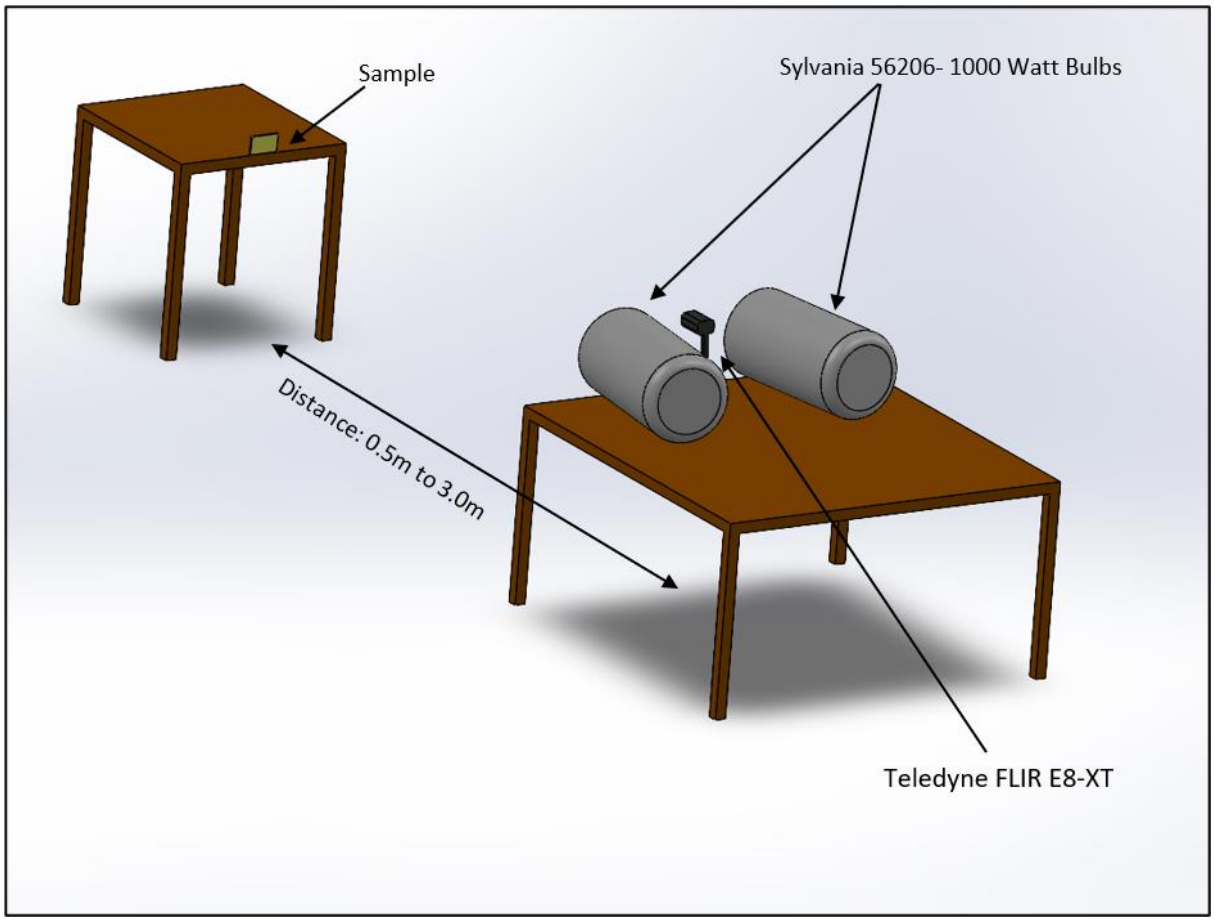

Figure 4: Theoretical setup of lights and sample.

2.4. Experimental Optimization

The optimization was conducted by heating the sample for 3 minutes at each distance, 0.5 m, 1.5 m, and 3.0 m, while continuously monitoring the temperature using a point and shoot

thermometer aimed at the center of the sample. Three tests were conducted per side, both front and back, to get a sufficient sample size to determine how long to run each test for. Undamaged samples were used during this test so that any potential defects would not affect the thermal data for the bulk sample.

After running the pilot test the temperatures of the front and back of the samples were plotted over the time the test was run. From the graphs of each of the tests, the optimal time to run each test was determined from the first time that both the front of the sample was heated 1 °C above the back, and the back was 1 °C warmer than the room temperature.

2.5. Procedure

Damaged samples were tested at 0.5 m, 1.5 m, and 3.0 m. When the samples were .5 m from the camera, they were heated for 10 s before a thermal image was captured. When at 1.5 m, the samples were heated for 30 s, and when at 3.0 m, the samples were heated for 45 s. These were the optimal times as determined by the optimization tests.

2.6. Damage Analysis

Images were uploaded onto the ImageJ program. Then, they were converted into 8-bit grayscale images. Finally, a threshold was applied to the image and the defects, if any were found, were able to be quantified. Doing this allows the program to differentiate between areas with a defect and areas that do not have defects.

3. Results

3.1. Experimental Optimization

From the optimization testing graphs data were produced for each distance. For the 0.5m tests, it was found that after 10 seconds the front of each sample was at least 1°C warmer than the back of the sample, and the back of each sample was at least 1°C warmer than the room temperature. The graphs for this are shown in Figure 5. It took the back of the samples longer to heat 1°C above room temperature for all samples than for the front of the sample to heat 1°C above the back of the sample.

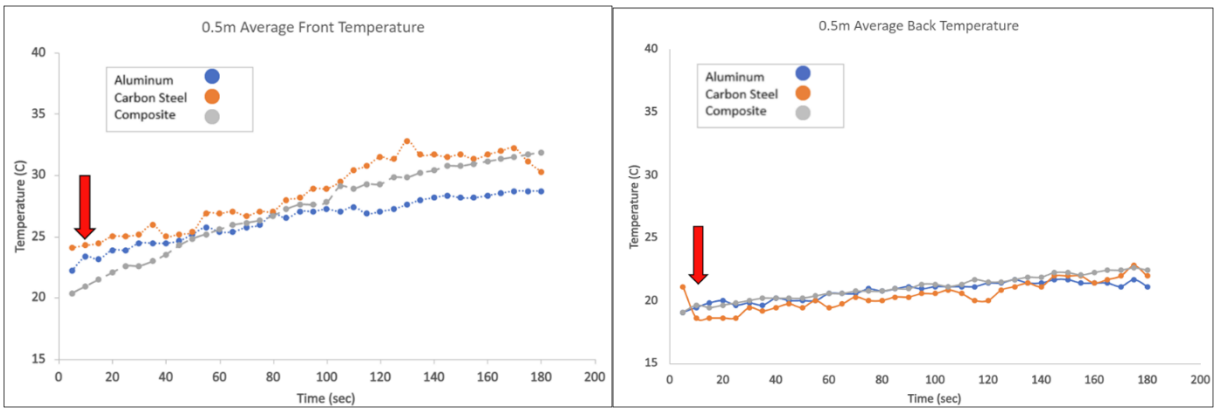

Figure 5: Temperature optimization graphs for 0.5 m test on front and back of samples.

At 1.5m the desired parameters were reached after 30 seconds, the graphs of this are shown in Figure 6. In this graph the composite sample heated a lot more than the metal samples. This is due to the emissivity of the composite sample being a lot lower than that of the metal samples.

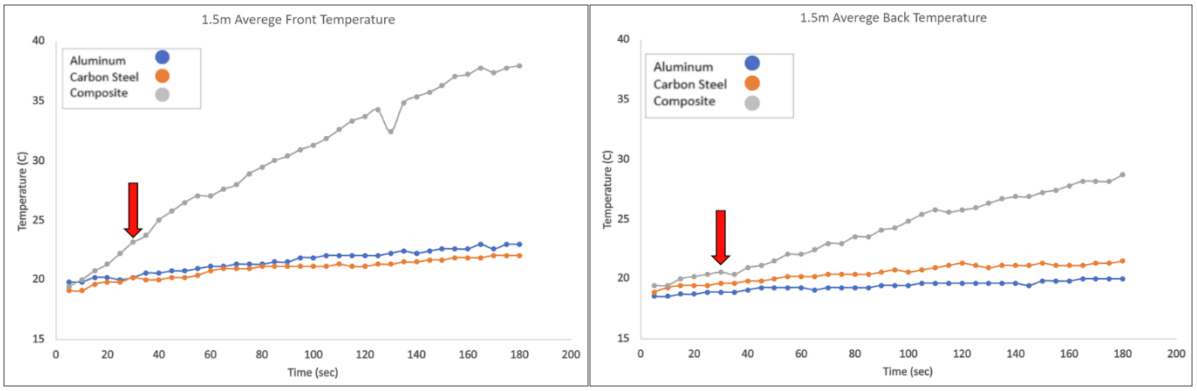

Figure 6: Temperature optimization graphs for 1.5 m test on front and back of samples.

From the 3.0m optimization test data, shown in Figure 7, it was determined that after 45 seconds the temperature increased enough to detect defects.

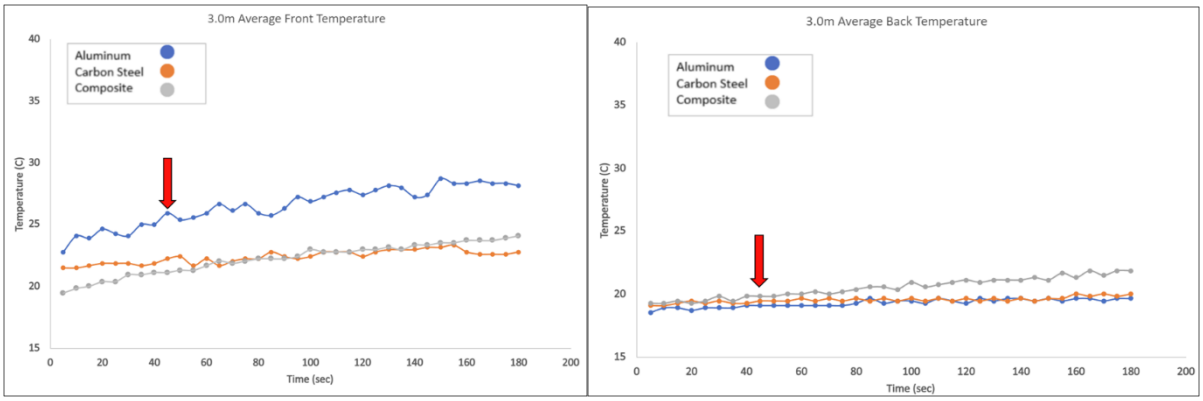

Figure 7: Temperature optimization graphs for 3.0 m test on front and back of samples.

3.2. Multi-system Damage Detection

3.2.1. Aluminum

The only damage present in the aluminum sample are two scratches along the diagonals of the face of the sample. These scratches are detectable via the raw thermograms at 0.5 m. These scratches heated up more than the bulk sample because the rough surface of the scratches scattered the light more than the bulk sample heating it up quicker than the rest of the sample, which allowed them to visible on thermographs, shown in Figure 8. However, at 1.5 m and 3.0 m, the defects are not detectable. They were not visible at these further distances because the sample was reflecting the heat from the lamps back into the thermal camera and overpowering any visible radiative heat from the sample. This prevented the detection of any thermal gradient on the sample. After running the images through ImageJ, the damage to the samples is detected only in the 0.5 m images, not at 1.5 m or at 3.0 m.

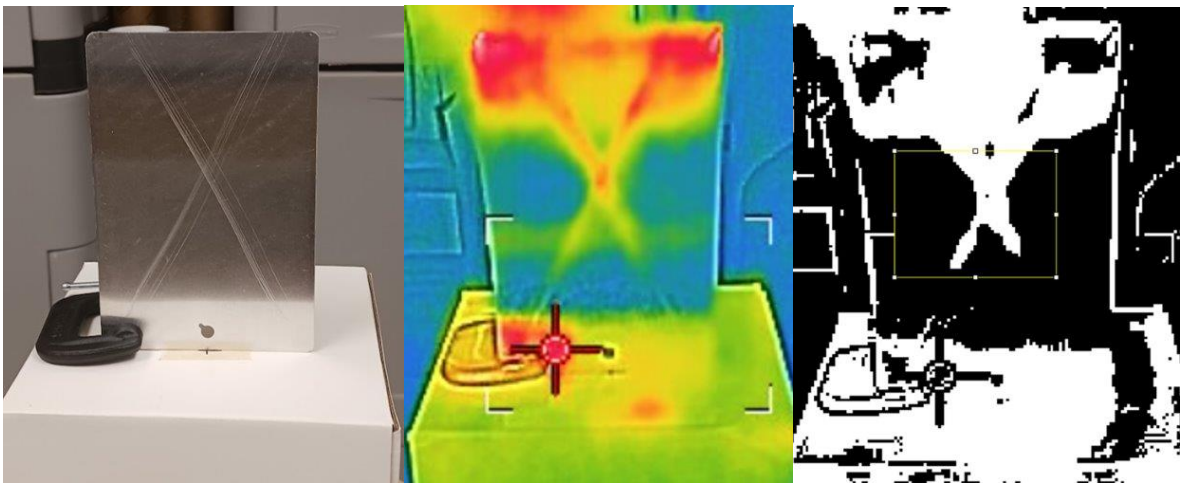

Figure 8: (l-r) Standard image of Al sample, raw thermograph taken at 0.5 m, and ImageJ processing of previous raw thermograph at 0.5 m.

3.2.2. Carbon Steel

In sample 1 of the carbon steel samples, the damage could be seen by observing the image. The only damage on this sample are two diagonal scratches forming an “X” shape on the sample, similar to the scratches present on the aluminum sample. These scratches were seen at .5 m on the raw thermograph however, they did not heat up as much compared to the aluminum sample. Since these scratches were smaller than those in the aluminum sample, they were not able to be detected by using Image J analysis, shown in Figure 9. No defects can be detected on the sample at 1.5 m and 3.0 m for sample 1 in either the raw thermographs or in the ImageJ analysis images. This is primarily because of the influence of reflection in the images like in the aluminum sample.

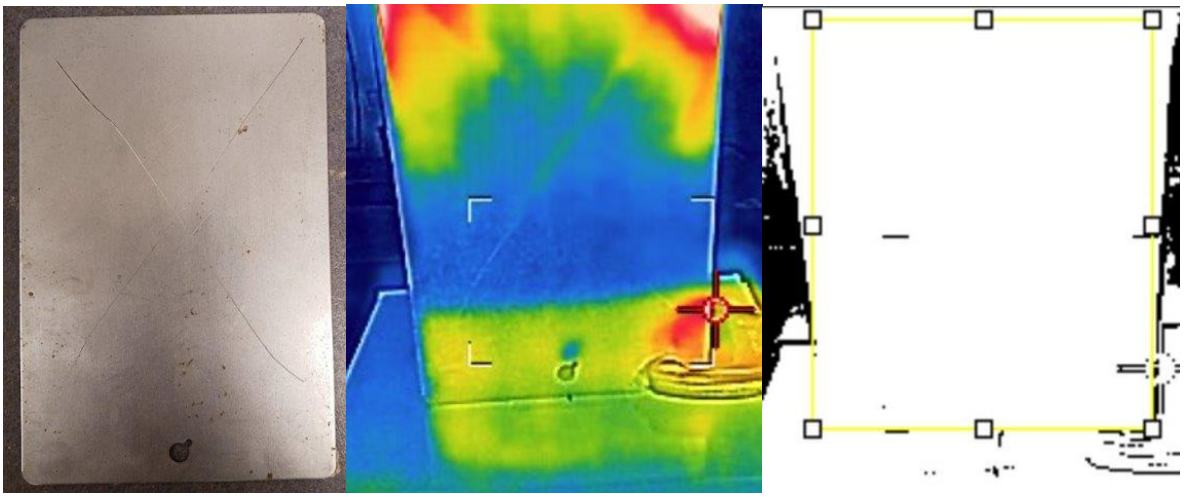

Figure 9: (l-r) Standard image of carbon steel sample 1, raw thermograph taken at 0.5 m, and ImageJ processing of previous raw thermograph at 0.5 m.

Sample 2 also showed defects on the .5 m tests, but they were faint and hardly recognizable on the raw thermograms. This resulted in ImageJ not being able to detect any defects in the sample. At 1.5 m and 3.0 m, the defects could not be seen on the raw thermograms due to reflection from the lights.

For sample 3, there was high oxidation on the surface which was able to be seen by a visual inspection. At .5 m, the thermograph showed the oxidation on the sample heating up more than the rest of the sample. This was also able to be shown through ImageJ analysis as the defects could be seen in those images, shown in Figure 10. However, at further distances of 1.5 m and 3.0 m no damage was able to be detected in the raw thermograms or in the ImageJ processing due to the reflection of the lights off the sample.

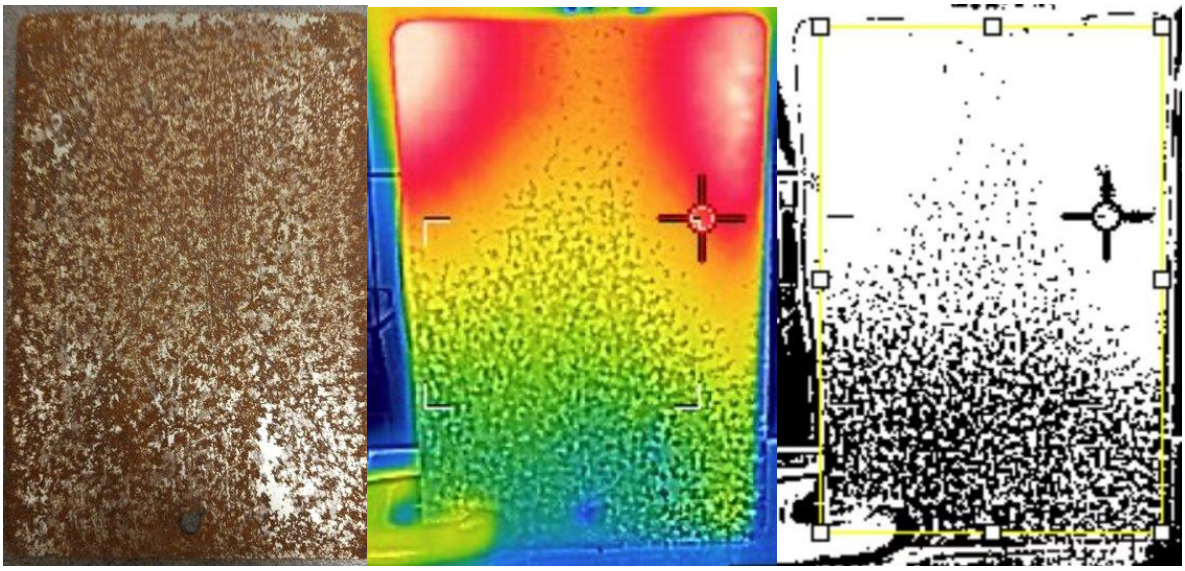

Figure 10: (l-r) Standard image of carbon steel sample 3, raw thermograph taken at 0.5 m, and ImageJ processing of previous raw thermograph at 0.5 m.

3.2.3. Composite

Delamination was able to be detected in the composite sample in the 0.5 m and 1.5 m tests. From the 0.5 m tests, it became clear that larger defects were easier to detect. Figure 11 shows some composite samples at 0.5 m following the test. In Figures 11A and 11B, the main limitation of using ImageJ can be seen. The bottom left portion of the sample in Figure 11A appears yellow and the defect appears light green. ImageJ was unable to detect a difference between these two colors and in the post image, Figure 11B, they are the same color.

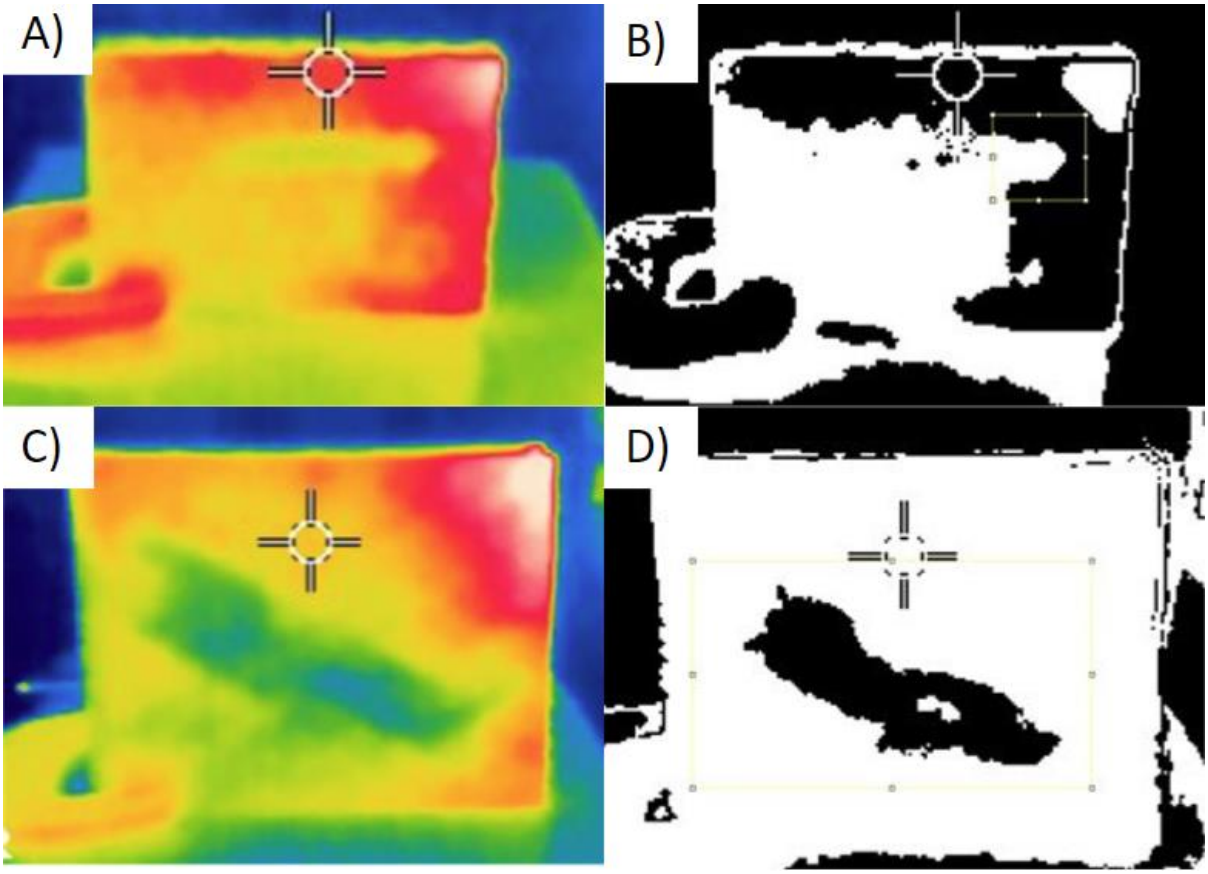

Figure 11: Composite samples tested at 0.5 m. A) Sample 1 raw thermograph. B) Sample 1 ImageJ processing. C) Sample 2 raw thermograph. D) Sample 2 ImageJ processing.

From the 1.5 m tests it became apparent that ImageJ detects defects in images best when the bulk of the sample is heated to a temperature that corresponds to a pink or white color in the raw thermograph, and the defect is heated to a temperature corresponding to a red or orange color on the raw thermograph. This can be seen in the samples present in Figure 12. Another limitation of ImageJ is that it is unable to accurately determine the size of the defects. Because the software goes by color when there is a color gradient transitioning from the bulk of the sample to the defect ImageJ must either register the transition in colors as black or white. This causes the size of the defect to be inaccurate due to the application of the gradient, and this can be seen between Figures 12C and 12D.

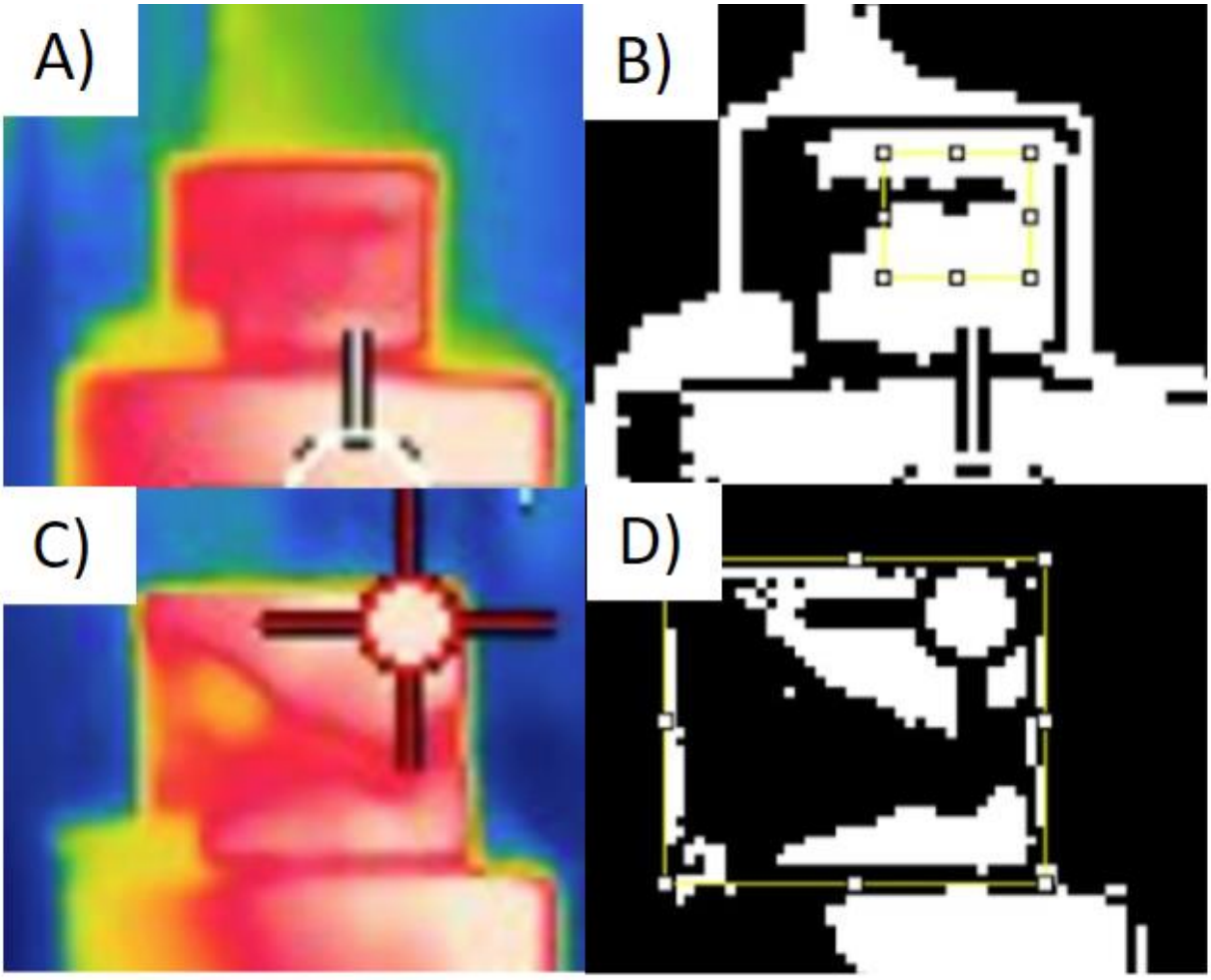

Figure 12: Composite samples tested at 1.5 m. A) Sample 1 raw thermograph. B) Sample 1 ImageJ processing. C) Sample 2 raw thermograph. D) Sample 2 ImageJ processing.

From the testing done at 3.0 m, damage was unable to be detected on the samples due to poor resolution from the thermal camera. Figure 13 shows the raw thermographs and the ImageJ images of samples 1 and 2. The images are very pixelated and grainy because of zooming into the images to make them fit the page.

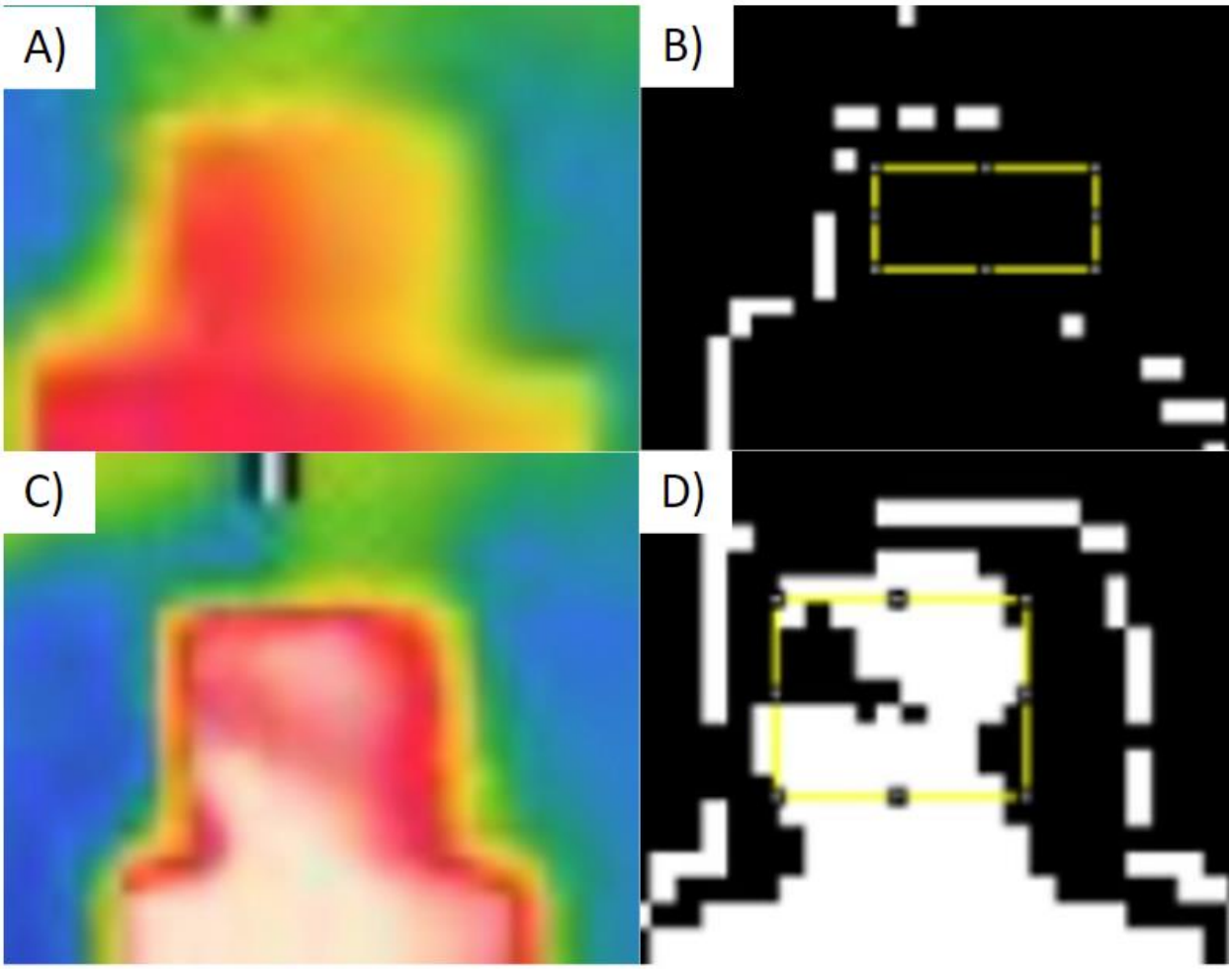

Figure 13: Composite samples tested at 3.0 m. A) Sample 1 raw thermograph. B) Sample 1 ImageJ processing. C) Sample 2 raw thermograph. D) Sample 2 ImageJ processing.

4. Discussion

During optimization testing, the composite sample heated much more than the metal samples during the 1.5 m tests. This trend was not present during the 0.5 m test because the lights at half a meter were focused on the edges of the sample, not the center. The composite sample does not diffuse heat as quickly as the metal samples so the center of the sample, where the thermometer was focused, heats more slowly. Also, the metal samples are thinner than the composite samples, with a higher surface area to volume ratio than the composites. This contributes to the metal samples not getting as hot. As the samples are heating up more of the heat is radiating off the back of the metal samples than in the composite sample. To verify that the thickness of the material is contributing to the samples retaining heat, in one test a Styrofoam back was added to an aluminum sample at 1.5 m, and it was heated for 30 s. After that time the temperature was measured, and it was found that the center of the sample was around 25 °C which was about the

temperature of the composite sample at that time and distance, showing that much of the heat is leaving through the back of the metal samples.

During the primary tests the metal samples at 0.5 m surface wear and oxidation were able to be detected. These results agree with other studies that were able to detect defects using long pulse thermography at similar distances [10]. For the composite samples tested at 0.5 m, delamination was able to be detected. These results agree with a study by Dattoma et. al [11]. Few studies have been conducted using long pulse thermography at distances greater than 0.5 m. Studies up to now have typically tested long pulse thermography at distances up to 0.5 m. In this test, it has been shown that it is possible to detect defects in composite materials at distances as far as 1.5 m.

Defects were unable to be detected in the metal samples at 1.5 m and 3.0 m. This was because the thermal camera was detecting reflected light from the 1000 W bulbs rather than the radiative heat emanating from the sample. Other studies have run into these problems, and they had several viable solutions to this problem. One approach was changing the position and the angle of the light so that the lights still heated the sample but reflected off directions away from the sample. This method was attempted by increasing the distance between the front of the lights from 40 cm to 100 cm causing the angle of the lights to also increase. Doing this did not cause enough of a change to produce a usable image at 1.5 m. It is likely that this could work if the distances and angles of the lights are increased further. However, if the lights are moved too far apart it is no longer practical to implement the system onto a drone.

Another way to reduce reflection that would likely work better with this project would be coating the metal samples with a compound with a lower reflectivity without altering the thermal properties of the sample.

At 3.0 m, the composite samples' defects were undetectable due to the resolution of the camera. The FLIR E8-XT thermal camera used in this experiment only has a resolution of 320x240 pixels. A better choice may be the FLIR X8580 camera which has a higher resolution of 1280x1024 pixels. This has about 4 times the resolution of the camera used in this experiment and would result in greater image clarity at further distances.

The ImageJ software used to detect defects was unable to distinguish the difference between some shades of yellow and green. A possible solution to this could be heating the samples longer. For the composite samples this would cause more of the sample to appear white and the defects to appear more red. Another solution is to find another image analysis software to detect defects. ImageJ was chosen for this project based on its ease of attainability, and ease of use. A more robust program can be developed to better suit this project's specific needs.

5. Conclusions

Long pulsed thermography was tested on 5005h24 aluminum, 1008 carbon steel and aramid fiber honeycomb sandwich structure composite samples at distances between 0.5 m and 3m. Defects were detected in the thermographs of the metal samples at 0.5 m. At further distances, the metal samples reflected too much heat from the lights to detect any defects. In the composite samples,

defects were detected in the thermographs as far as 1.5 m away from the lights. At 3.0 m the defects were not detectable in the composites due to the resolution of the camera.

It is not recommended to implement this testing method onto drones for the evaluation of material defects aboard naval ships. Since the drones will have to fly at a distance of at most 0.5 m away from the ship, this can risk damage to the ship and the drone itself if it flies only 0.5 m away. Even at the maximum successful distances of 1.5 m for the composites, it can still risk flying too close to the ship. In addition, the two 1000 W lights needed to heat the samples being tested require much more power than is available for most commercial drones. This would lead to a reduced amount of time that the drone can be used to image the ship. Also, the weight of the lights would require a more powerful drone, further reducing the amount of time that the drone could potentially be in the air due to the larger required battery to power this type of potential drone.

If further studies are conducted using long pulsed thermography, there are a few considerations that should be made. The metal samples should be coated or painted to reduce the amount of reflection of heat seen from the lights off the sample at further distances. A higher resolution camera, like the FLIR X8580, will result in increased defect detection on the composite samples. Using image analysis software that can better differentiate between colors produced by the thermographs, especially green and yellow, will result in better results from thermal image analysis. Outdoor testing should also be considered because this technology will be used outside to analyze ships and should be tested both during the day and the night to determine its viability in the field.

6. References

[1] Doshvarpassand, Siavash, et al. “An Overview of Corrosion Defect Characterization Using Active Infrared Thermography.” *Infrared Physics & Technology*, vol. 96, Elsevier B.V, 2019, pp. 366–89, https://doi.org/10.1016/j.infrared.2018.12.006.

[2] Wang, Zijun, et al. “Image Processing Based Quantitative Damage Evaluation in Composites with Long Pulse Thermography.” *NDT & E International : Independent Nondestructive Testing and Evaluation*, vol. 99, Elsevier Ltd, 2018, pp. 93–104, https://doi.org/10.1016/j.ndteint.2018.07.004.

[3]Almond, Darryl P., et al. “Long Pulse Excitation Thermographic Non-Destructive Evaluation.” *NDT & E International : Independent Nondestructive Testing and Evaluation*, vol. 87, Elsevier Ltd, 2017, pp. 7–14, https://doi.org/10.1016/j.ndteint.2017.01.003.

[4] “Pros and Cons of Carbon Steel: What You Should Know” *Monroe*, 2018, https://monroeengineering.com/blog/pros-and-cons-of-carbon-steel-what-you-should-know/.

[5] “Corrosion and Corrosion Prevention” *ECS*, https://www.electrochem.org/corrosion-science.

[6] Jönsson, M., et al. “The Use of Infrared Thermography in the Corrosion Science Area: The Use of Infrared Thermography in Corrosion Science.” *Materials and Corrosion*, vol. 61, no. 11, 2010, pp. 961–65, https://doi.org/10.1002/maco.200905525.

[7] Mallick, P. K. “Fiber-Reinforced Composites : Materials, Manufacturing, and Design” . 3rd ed., [expanded and rev. ed.]., CRC Press, 2008.

[8] “INFRARED CAMERA WITH MSX & WI-FI: FLIR Ex-Series” *FLIR*, https://www.testequipmentdepot.com/flir/pdf/ex-xt-series_datasheet.pdf

[9] Pierce, James, and Nathan B. Crane. “Impact of Pulse Length on the Accuracy of Defect Depth Measurements in Pulse Thermography.” *Journal of Heat Transfer*, vol. 141, no. 4, ASME, 2019, https://doi.org/10.1115/1.4042785.

[10] Broberg, Patrik. “Surface Crack Detection in Welds Using Thermography.” NDT & E International : Independent Nondestructive Testing and Evaluation, vol. 57, Elsevier Ltd, 2013, pp. 69–73, https://doi.org/10.10

16/j.ndteint.2013.03.008.

[11] Dattoma, V., et al. “Thermographic Investigation of Sandwich Structure Made of Composite Material.” *NDT & E International : Independent Nondestructive Testing and Evaluation*, vol. 34, no. 8, Elsevier Ltd, 2001, pp. 515–20, https://doi.org/10.1016/S0963-8695(00)00082-7.

7. Appendix

Table I: Optimization test data for 0.5 m.

.5 meters							
Time	Aluminum		Carbon Steel		Composite		
	average front	Average Back	Front average	Back average	avg front temp	avg back temp	Camera test data
5	22.224	19.0756	24.076	21.1128	20.372	19.0756	Al
10	23.3352	19.446	24.2612	18.6126	20.9276	19.6312	20.52129
15	23.15	19.8164	24.4464	18.6126	21.4832	19.446	CS2
20	23.8908	20.0016	25.002	18.6126	22.0388	19.6312	22.13002
25	23.8908	19.6312	25.002	18.6126	22.5944	19.8164	CO2
30	24.4464	19.8164	25.1872	19.446	22.5944	20.0016	21.4234
35	24.4464	19.6312	25.928	19.1682	22.9648	20.1868	
40	24.4464	20.1868	25.002	19.446	23.5204	20.1868	
45	24.6316	20.0016	25.1872	19.7238	24.2612	20.1868	
50	25.1872	20.0016	25.3724	19.446	24.8168	20.1868	
55	25.7428	20.0016	26.854	20.0016	25.1872	20.372	
60	25.3724	20.5572	26.854	19.446	25.5576	20.5572	
65	25.3724	20.5572	27.0392	19.7238	25.928	20.5572	
70	25.7428	20.5572	26.6688	20.2794	26.1132	20.7424	
75	25.928	20.9276	27.0392	20.0016	26.2984	20.7424	
80	26.854	20.7424	27.0392	20.0016	26.6688	20.7424	
85	26.4836	20.9276	27.9652	20.2794	27.2244	20.9276	
90	27.0392	21.1128	28.1504	20.2794	27.5948	20.9276	
95	27.0392	20.9276	28.8912	20.5572	27.5948	21.298	
100	27.2244	21.1128	28.8912	20.5572	27.78	21.298	
105	27.0392	21.1128	29.4468	20.835	29.0764	21.1128	
110	27.4096	21.1128	30.3728	20.5572	28.8912	21.298	
115	26.854	21.1128	30.7432	20.0016	29.2616	21.6684	
120	27.0392	21.3906	31.484	20.0016	29.2616	21.4832	
125	27.2244	21.3906	31.2988	20.835	29.8172	21.4832	
130	27.5948	21.6684	32.7804	21.1128	29.8172	21.6684	
135	27.9652	21.3906	31.6692	21.3906	30.1876	21.8536	
140	28.1504	21.3906	31.6692	21.1128	30.3728	21.8536	
145	28.3356	21.6684	31.484	21.9462	30.7432	22.224	
150	28.1504	21.6684	31.6692	21.9462	30.7432	22.224	
155	28.1504	21.3906	31.2988	21.9462	30.9284	22.0388	
160	28.3356	21.3906	31.6692	21.3906	31.1136	22.224	
165	28.5208	21.3906	31.947	21.6684	31.2988	22.4092	
170	28.706	21.1128	32.2248	21.9462	31.484	22.4092	
175	28.706	21.6684	31.1136	22.7796	31.6692	22.5944	
180	28.706	21.1128	30.2802	21.9462	31.8544	22.4092	

Table II: Optimization test data for 1.5 m.

1.5 Meter							
Time	Aluminum		Carbon Steel		Composite		
	average fr	Average B	Front aver	Back aver	avg front t	avg back t	Camera test data
5	19.8164	18.52	19.0756	18.8904	19.446	19.446	Al
10	19.8164	18.52	19.0756	19.2608	20.0016	19.446	18.89074
15	20.1868	18.7052	19.6312	19.446	20.7424	20.0016	CS
20	20.1868	18.7052	19.8164	19.446	21.298	20.1868	22.77856
25	20.0016	18.8904	19.8164	19.446	22.224	20.372	CO
30	20.1868	18.8904	20.1868	19.6312	23.15	20.5572	24.48881
35	20.5572	18.8904	20.0016	19.6312	23.7056	20.372	
40	20.5572	19.0756	20.0016	19.8164	25.002	20.9276	
45	20.7424	19.2608	20.1868	19.8164	25.7428	21.1128	
50	20.7424	19.2608	20.1868	20.0016	26.4836	21.4832	
55	20.9276	19.2608	20.372	20.1868	27.0392	22.0388	
60	21.1128	19.2608	20.7424	20.1868	27.0392	22.0388	
65	21.1128	19.0756	20.9276	20.1868	27.5948	22.4092	
70	21.298	19.2608	20.9276	20.372	27.9652	22.9648	
75	21.298	19.2608	20.9276	20.372	28.8912	22.9648	
80	21.298	19.2608	21.1128	20.372	29.4468	23.5204	
85	21.4832	19.2608	21.1128	20.372	30.0024	23.5204	
90	21.4832	19.446	21.1128	20.5572	30.3728	24.076	
95	21.8536	19.446	21.1128	20.7424	30.9284	24.2612	
100	21.8536	19.446	21.1128	20.5572	31.2988	24.8168	
105	22.0388	19.6312	21.1128	20.7424	31.8544	25.3724	
110	22.0388	19.6312	21.298	20.9276	32.5952	25.7428	
115	22.0388	19.6312	21.1128	21.1128	33.336	25.5576	
120	22.0388	19.6312	21.1128	21.298	33.7064	25.7428	
125	22.0388	19.6312	21.298	21.1128	34.262	25.928	
130	22.224	19.6312	21.298	20.9276	32.41	26.2984	
135	22.4092	19.6312	21.4832	21.1128	34.8176	26.6688	
140	22.224	19.6312	21.4832	21.1128	35.3732	26.854	
145	22.4092	19.446	21.6684	21.1128	35.7436	26.854	
150	22.5944	19.8164	21.6684	21.298	36.2992	27.2244	
155	22.5944	19.8164	21.8536	21.1128	37.04	27.4096	
160	22.5944	19.8164	21.8536	21.1128	37.2252	27.78	
165	22.9648	20.0016	21.8536	21.1128	37.7808	28.1504	
170	22.5944	20.0016	22.0388	21.298	37.4104	28.1504	
175	22.9648	20.0016	22.0388	21.298	37.7808	28.1504	
180	22.9648	20.0016	22.0388	21.4832	37.966	28.706	

Table III: Optimization Test Data for 3.0 m.

3.0 Meter							
Time	Aluminum		Carbon Steel		Composite		
	average fr	Average B	Front aver	Back aver	avg front t	avg back t	Camera test data
5	22.7796	18.52	21.4832	19.0756	19.446	19.2608	Al
10	24.076	18.8904	21.4832	19.0756	19.8164	19.2608	25.26971
15	23.8908	18.8904	21.6684	19.2608	20.0016	19.446	CS
20	24.6316	18.7052	21.8536	19.446	20.372	19.2608	22.60069
25	24.2612	18.8904	21.8536	19.2608	20.372	19.446	CO
30	24.076	18.8904	21.8536	19.446	20.9276	19.8164	21.81788
35	25.002	18.8904	21.6684	19.2608	20.9276	19.446	
40	25.002	19.0756	21.8536	19.2608	21.1128	19.8164	
45	25.928	19.0756	22.224	19.446	21.1128	19.8164	
50	25.3724	19.0756	22.4092	19.446	21.298	19.8164	
55	25.5576	19.0756	21.6684	19.446	21.298	20.0016	
60	25.928	19.0756	22.224	19.6312	21.6684	20.0016	
65	26.6688	19.0756	21.6684	19.446	22.0388	20.1868	
70	26.1132	19.0756	22.0388	19.6312	21.8536	20.0016	
75	26.6688	19.0756	22.224	19.446	22.0388	20.1868	
80	25.928	19.2608	22.224	19.6312	22.224	20.372	
85	25.7428	19.6312	22.7796	19.446	22.224	20.5572	
90	26.2984	19.2608	22.4092	19.6312	22.224	20.5572	
95	27.2244	19.446	22.224	19.446	22.4092	20.372	
100	26.854	19.446	22.4092	19.6312	22.9648	20.9276	
105	27.2244	19.2608	22.7796	19.446	22.7796	20.5572	
110	27.5948	19.6312	22.7796	19.6312	22.7796	20.7424	
115	27.78	19.446	22.7796	19.446	22.7796	20.9276	
120	27.4096	19.2608	22.4092	19.6312	22.9648	21.1128	
125	27.78	19.6312	22.7796	19.446	22.9648	20.9276	
130	28.1504	19.446	22.9648	19.6312	23.15	21.1128	
135	27.9652	19.6312	22.9648	19.446	22.9648	21.1128	
140	27.2244	19.6312	22.9648	19.6312	23.3352	21.1128	
145	27.4096	19.446	23.15	19.446	23.3352	21.298	
150	28.706	19.6312	23.15	19.6312	23.5204	21.1128	
155	28.3356	19.446	23.3352	19.6312	23.5204	21.6684	
160	28.3356	19.6312	22.7796	20.0016	23.7056	21.298	
165	28.5208	19.6312	22.5944	19.8164	23.7056	21.8536	
170	28.3356	19.446	22.5944	20.0016	23.7056	21.4832	
175	28.3356	19.6312	22.5944	19.8164	23.8908	21.8536	
180	28.1504	19.6312	22.7796	20.0016	24.076	21.8536	

Aluminum sample thermographs and ImageJ images at 0.5 m.

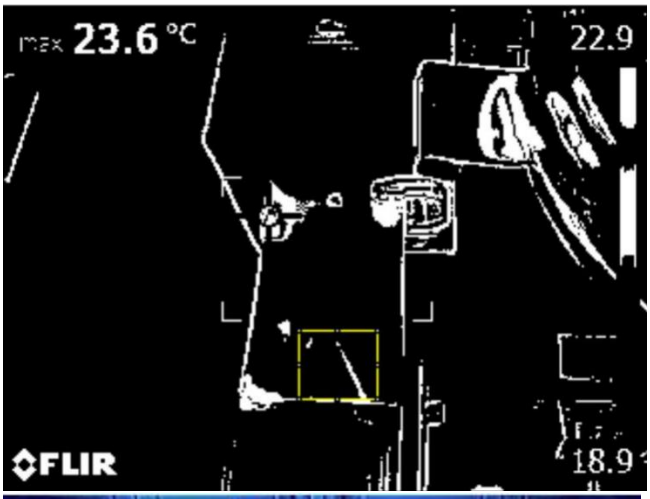
max 23.6 °C
22.9
FLIR
18.9


max ~33.4 °C
33.6
FLIR
20.8

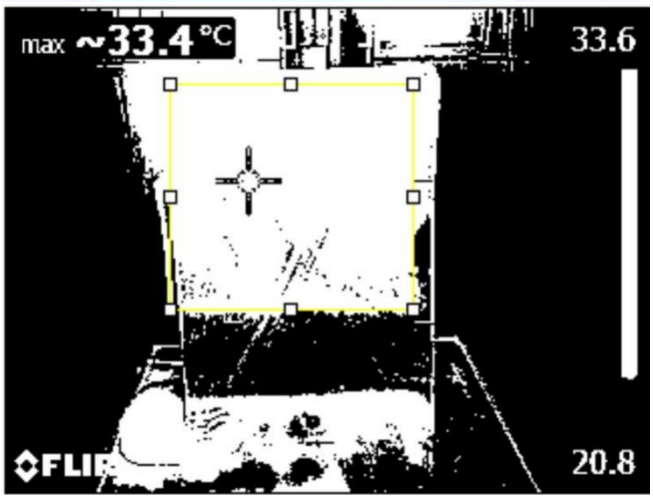
max ~33.4 °C
33.6
FLIR
20.8

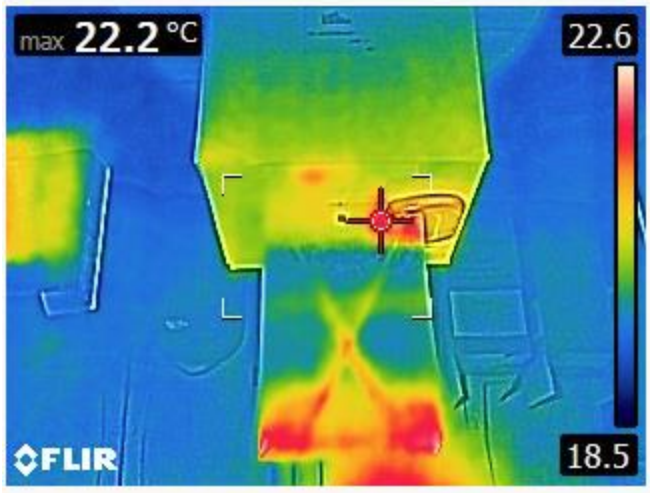

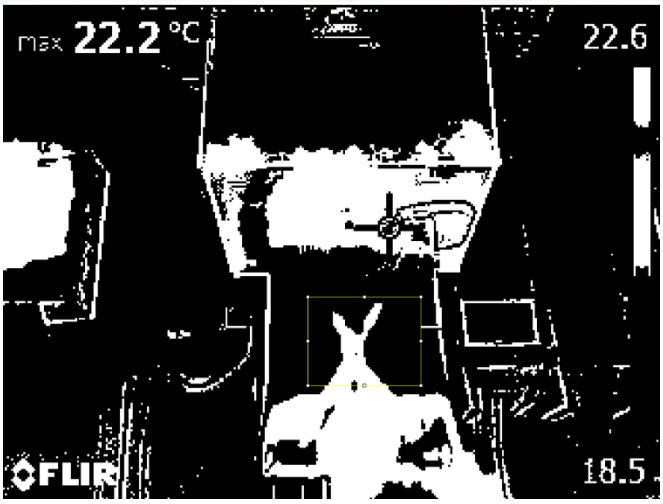

Aluminum sample thermographs and ImageJ images at 1.5 m.

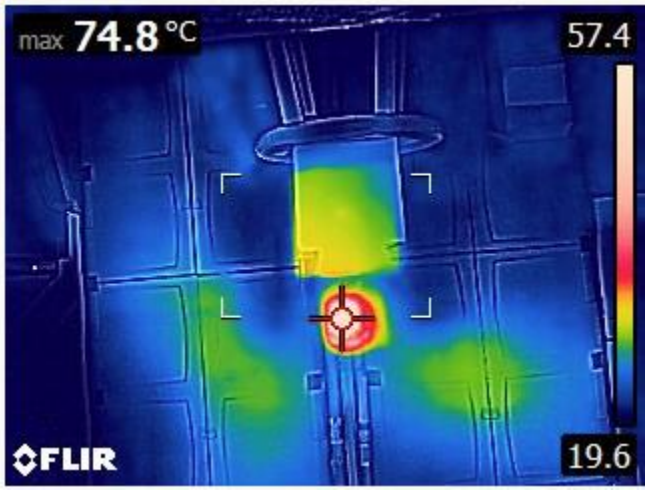

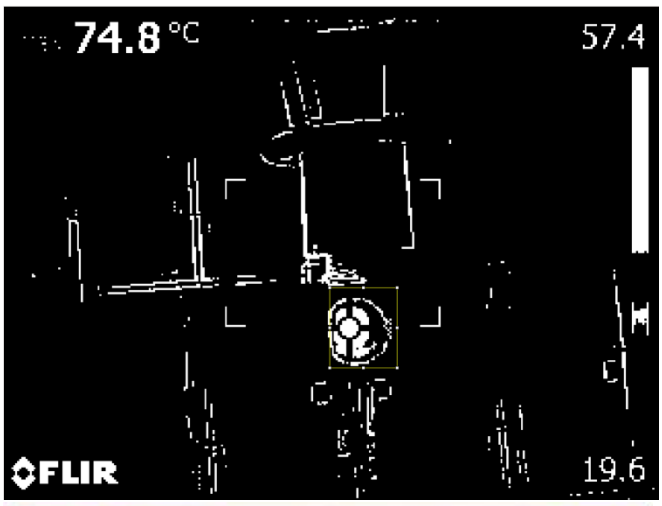
74.8 °C
57.4
FLIR
19.6

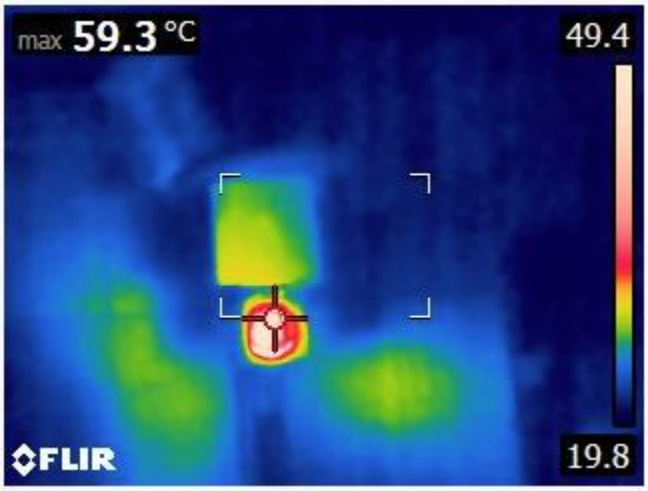
max 59.3 °C
49.4
FLIR
19.8

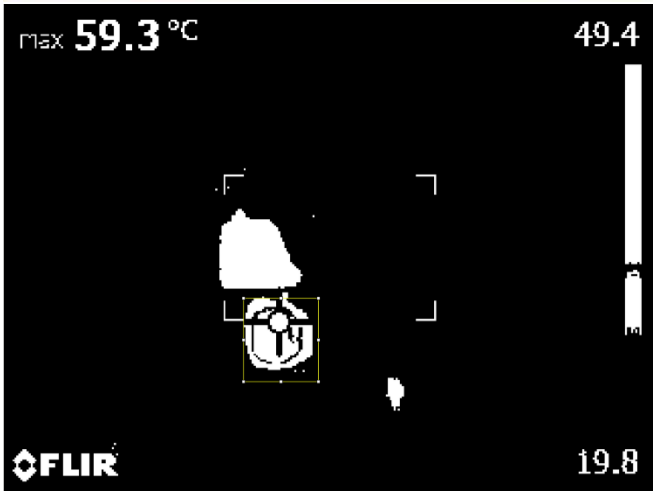
max 59.3 °C
49.4
FLIR
19.8

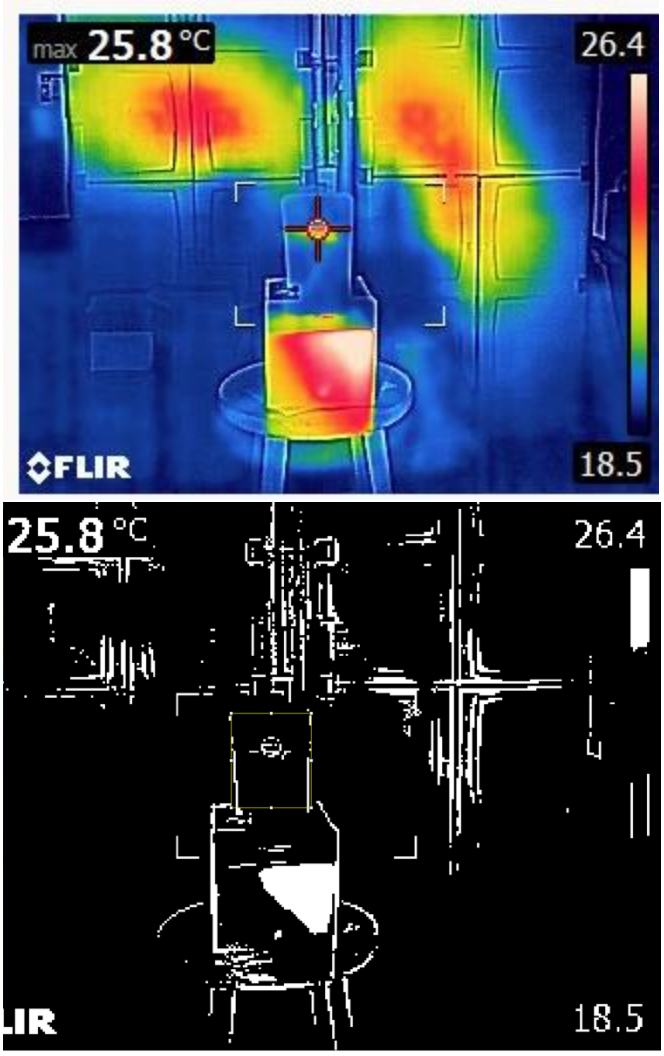

Aluminum sample thermographs and ImageJ images at 3.0 m.

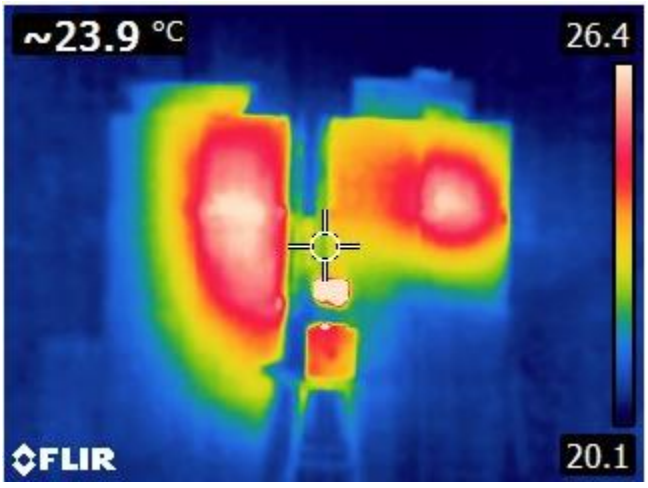

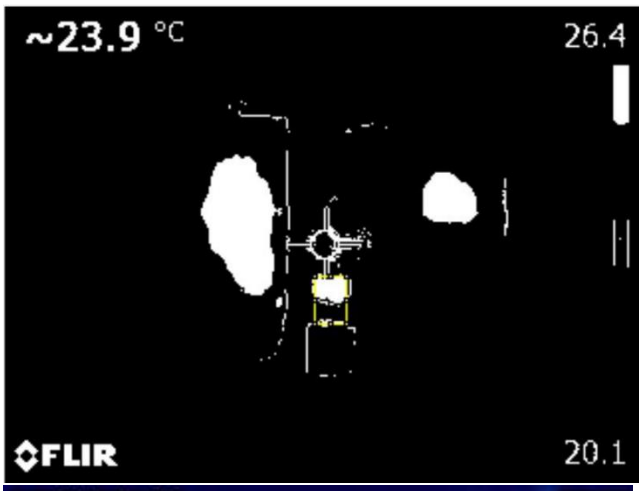
~23.9 °C
26.4
FLIR
20.1


~23.0 °C
28.3
FLIR
19.1

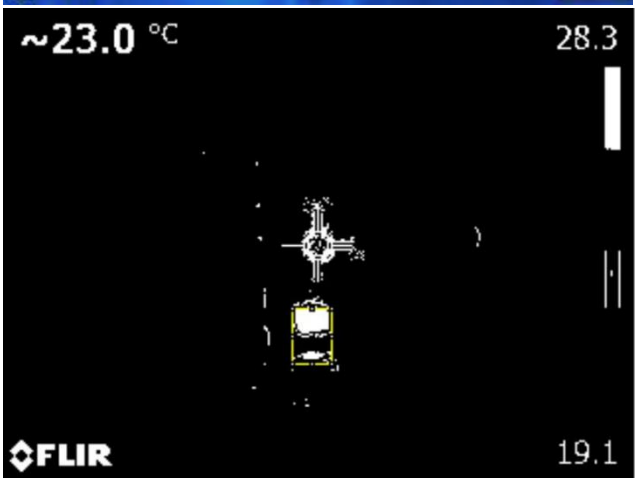
~23.0 °C
28.3
FLIR
19.1

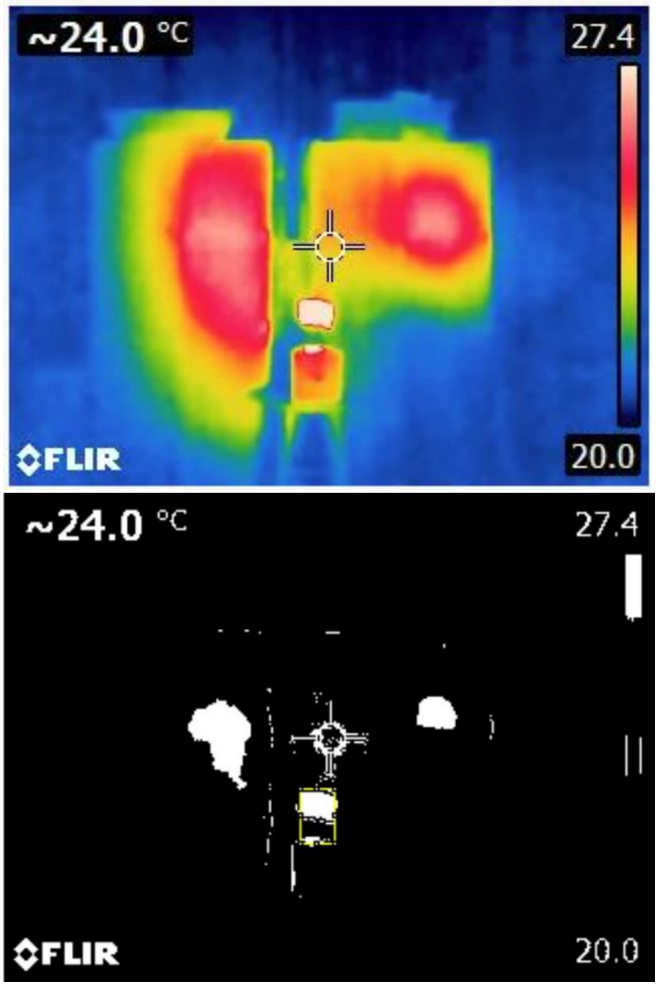

Carbon steel thermographs and ImageJ images at 0.5 m.
Sample 1

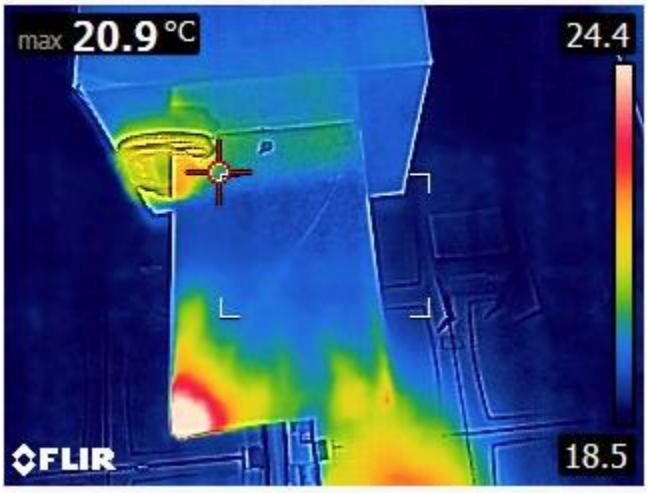

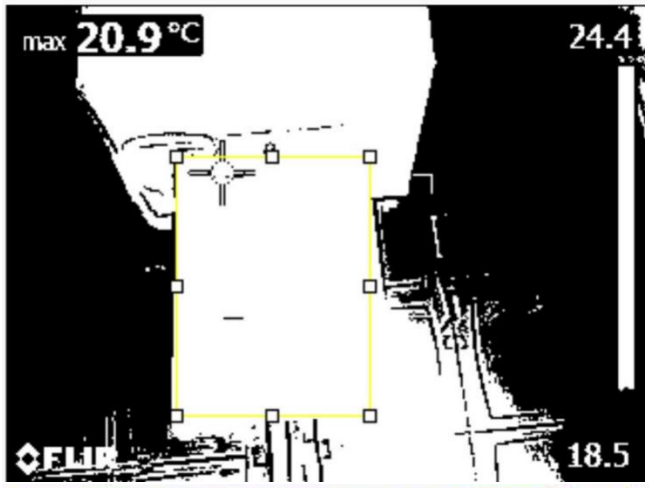
max 20.9 °C
24.4
FLIR
18.5

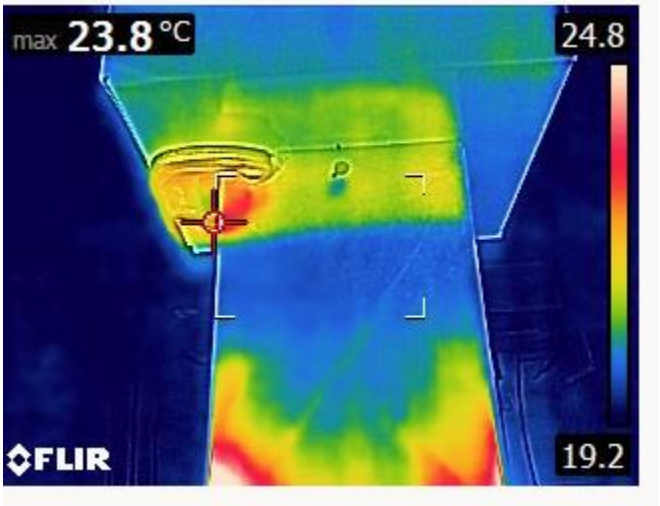
max 23.8 °C
24.8
FLIR
19.2

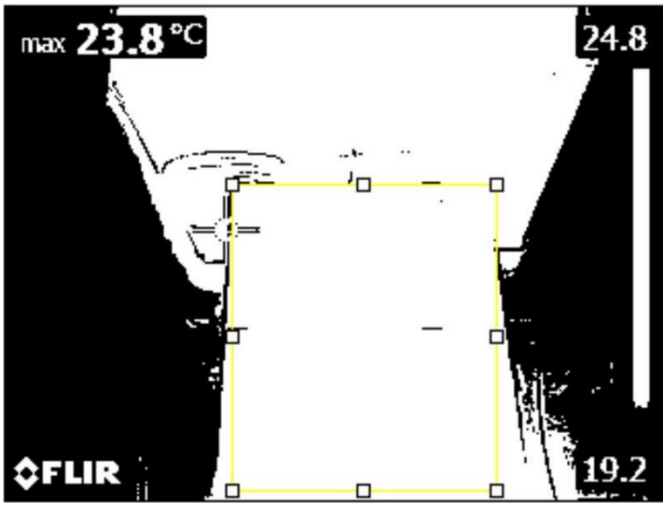
max 23.8 °C
24.8
FLIR
19.2


max ~23.3 °C
30.3
FLIR
20.4

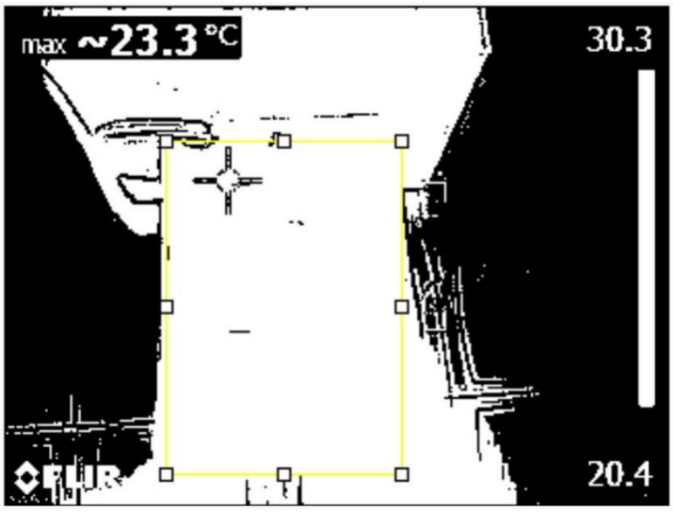
max ~23.3 °C
30.3
FLIR
20.4

Sample 2


max 25.9 °C
28.5
FLIR
19.2

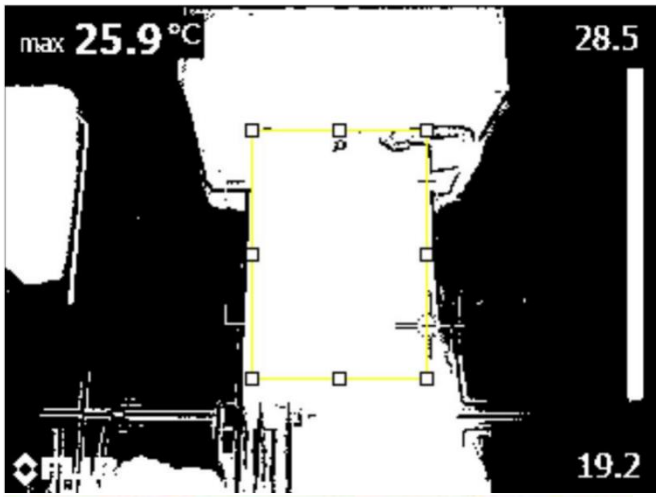
max 25.9 °C
28.5
19.2

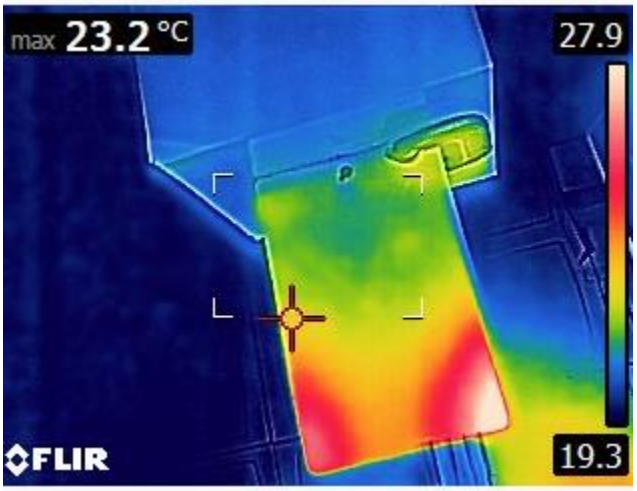
max 23.2 °C
27.9
FLIR
19.3

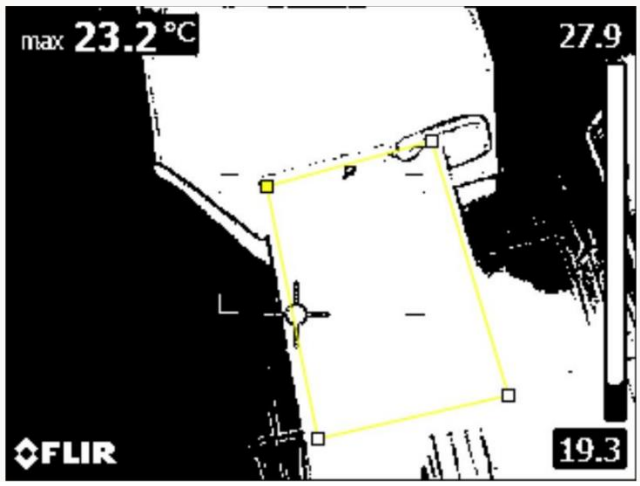
max 23.2 °C
27.9
FLIR
19.3

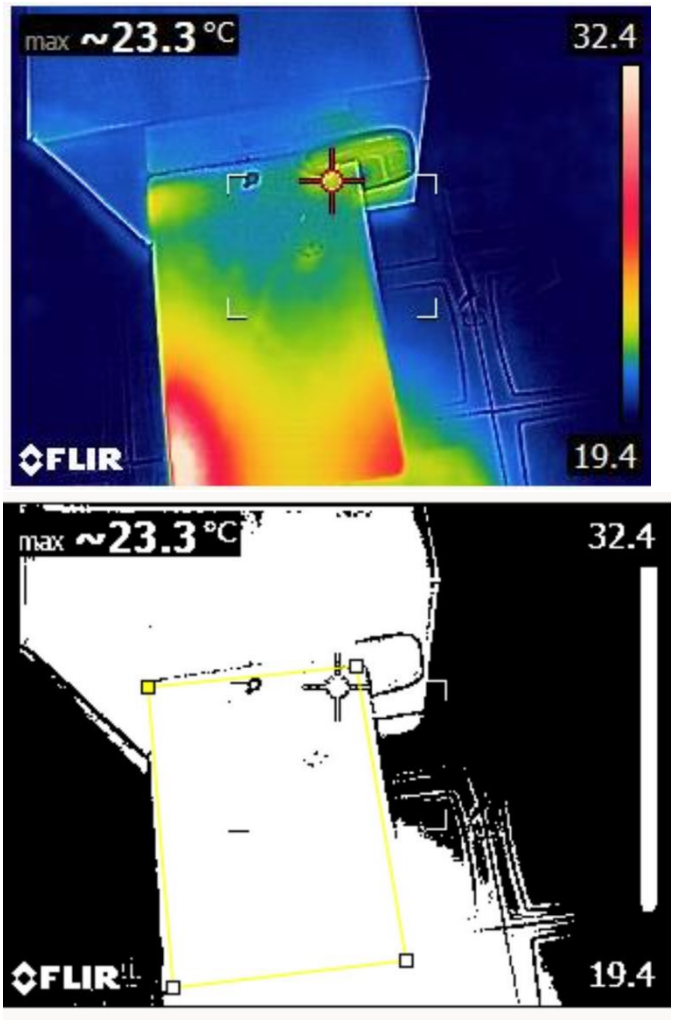

Sample 3

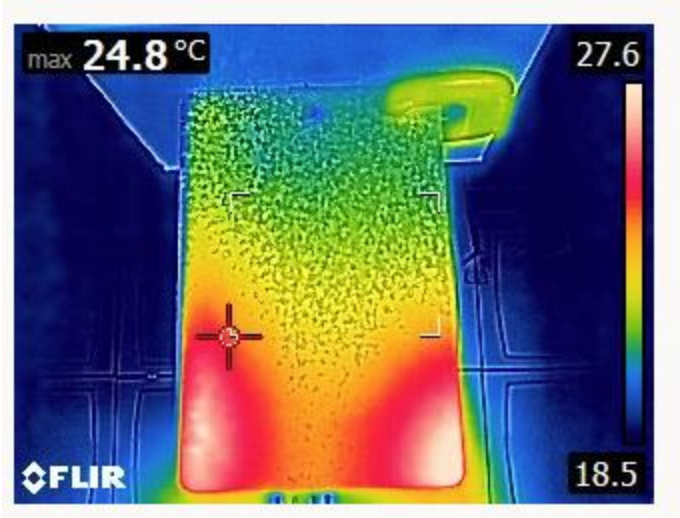
max 24.8 °C
27.6
FLIR
18.5

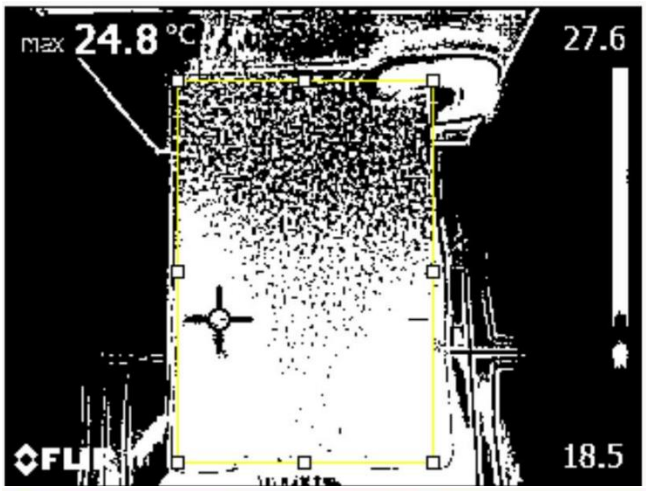
max 24.8 °C
27.6
18.5


max ~25.7 °C
28.2
FLIR
20.0

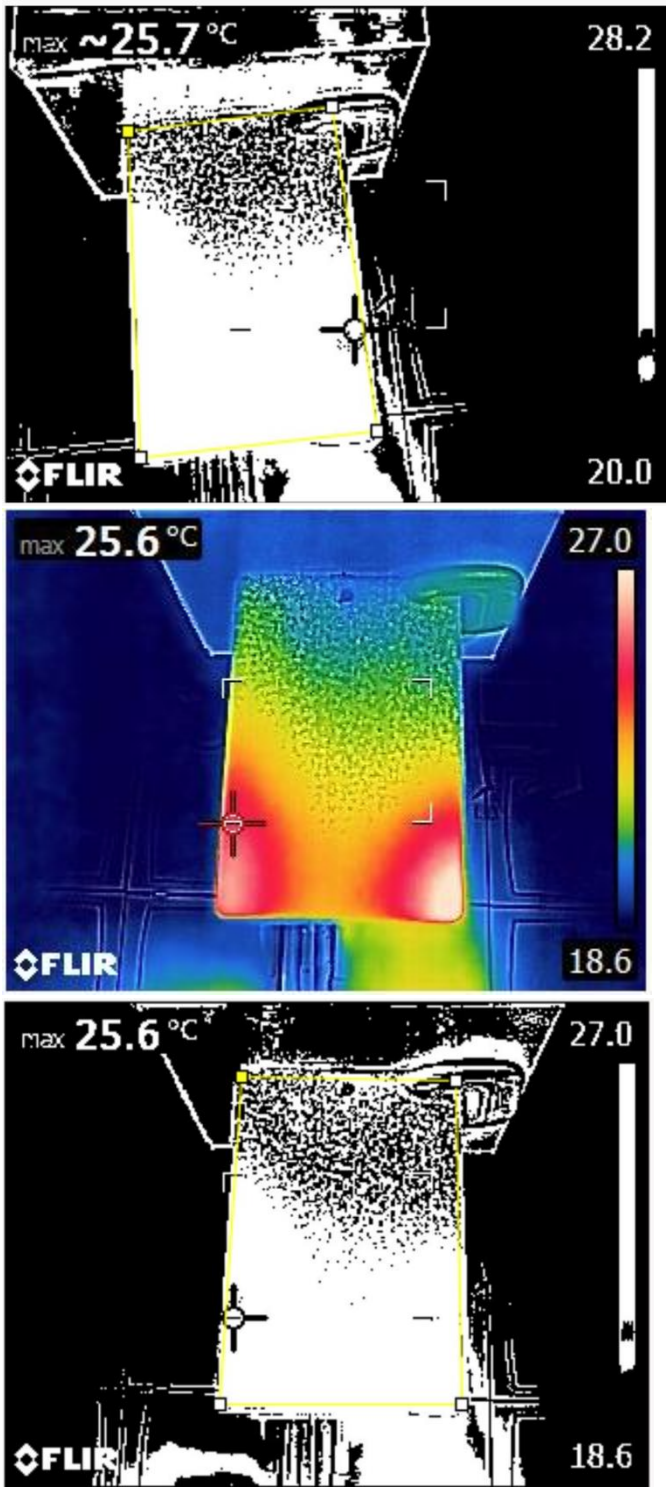

Carbon steel thermographs and ImageJ images at 1.5 m.
Sample 1


max 28.2 °C
26.5
FLIR
19.0

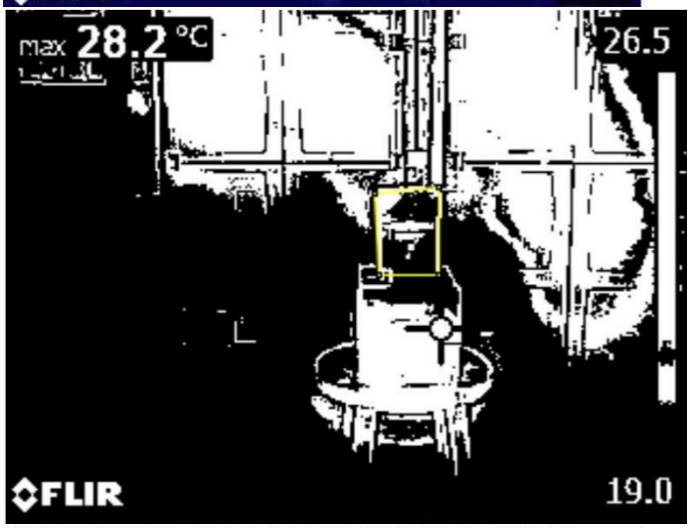
max 28.2 °C
26.5
FLIR
19.0

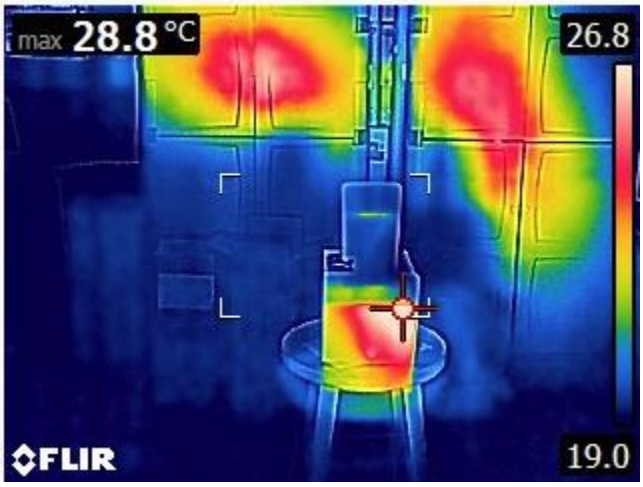
max 28.8 °C
26.8
FLIR
19.0

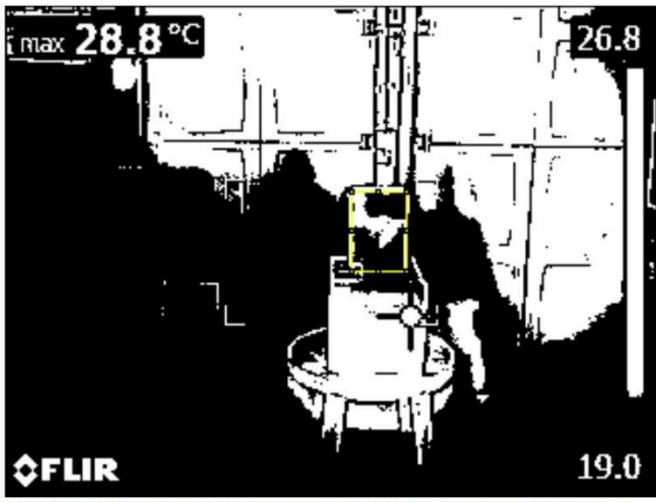
max 28.8 °C
26.8
FLIR
19.0


max ~60.1 °C
37.7
FLIR
20.3

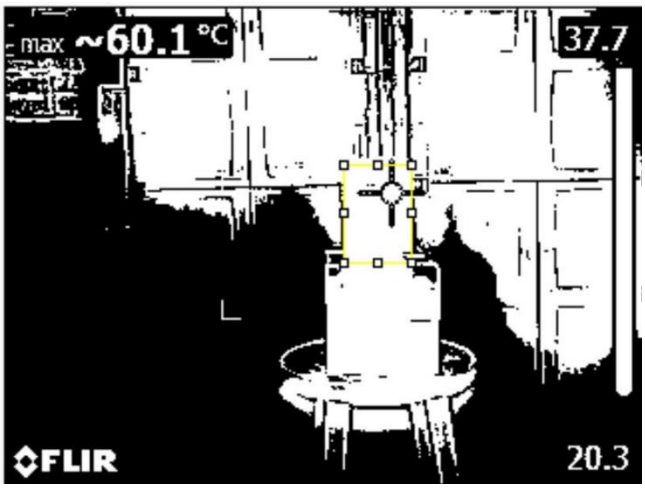
max ~60.1 °C
37.7
FLIR
20.3

Sample 2


max 28.7 °C
31.7
19.6
FLIR

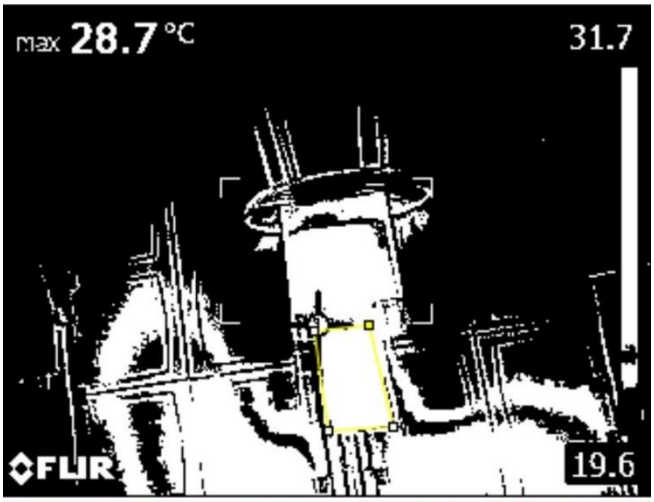
max 28.7 °C
31.7
19.6
FLIR

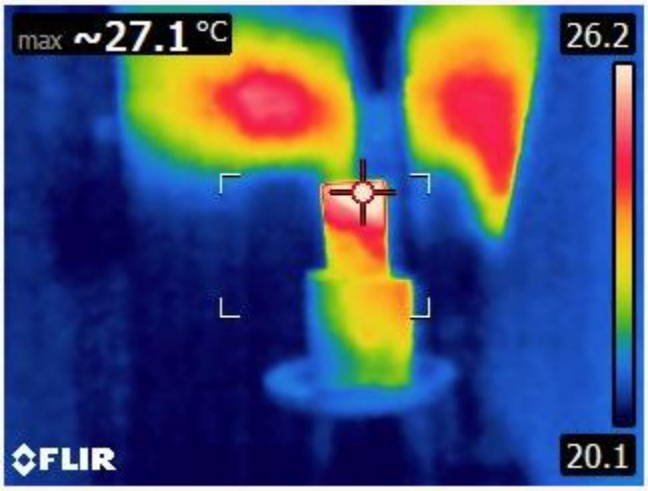
max ~27.1 °C
26.2
20.1
FLIR

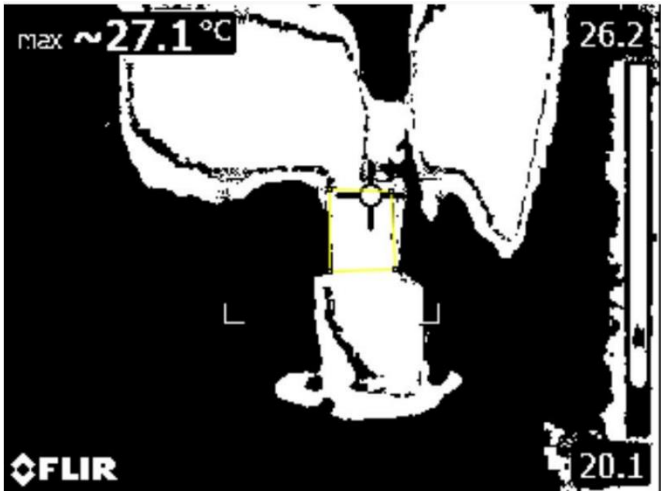
max ~27.1 °C
26.2
20.1
FLIR

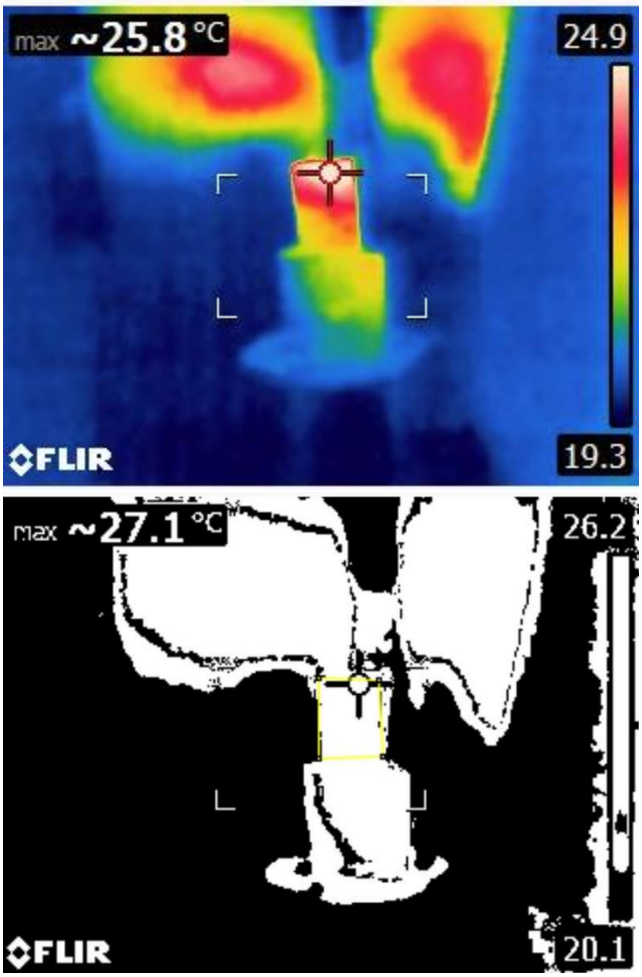

Sample 3


max 34.5 °C
30.8
FLIR
19.7

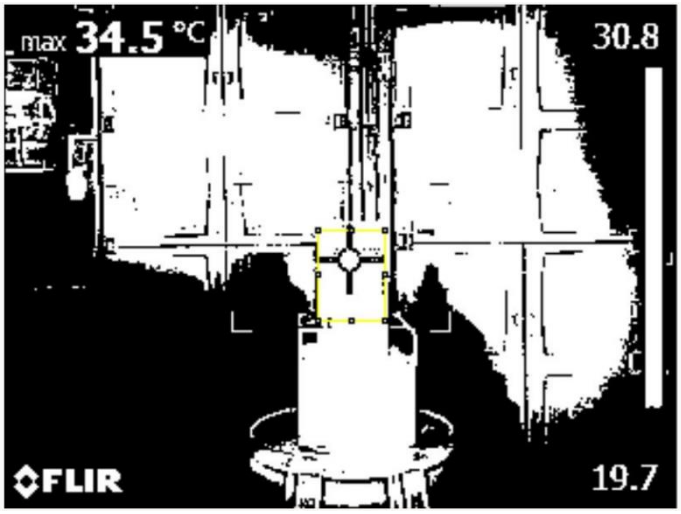
max 34.5 °C
30.8
FLIR
19.7

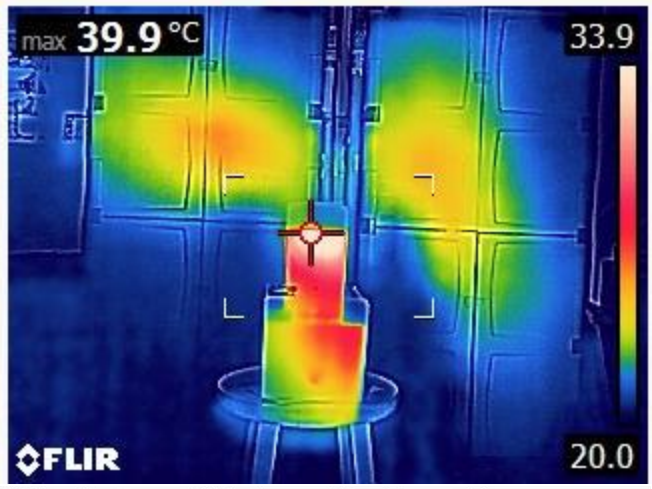
max 39.9 °C
33.9
FLIR
20.0

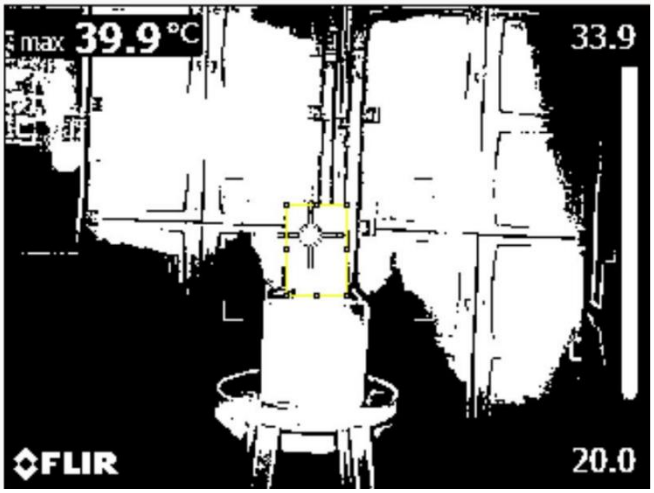
max 39.9 °C
33.9
FLIR
20.0

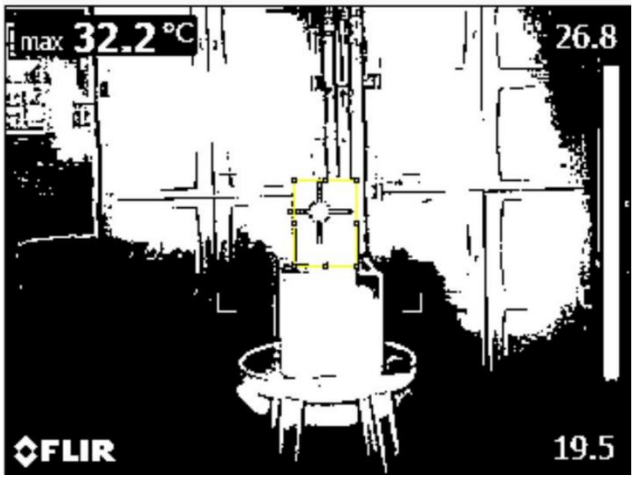

Carbon steel thermographs and ImageJ images at 3.0 m.
Sample 1

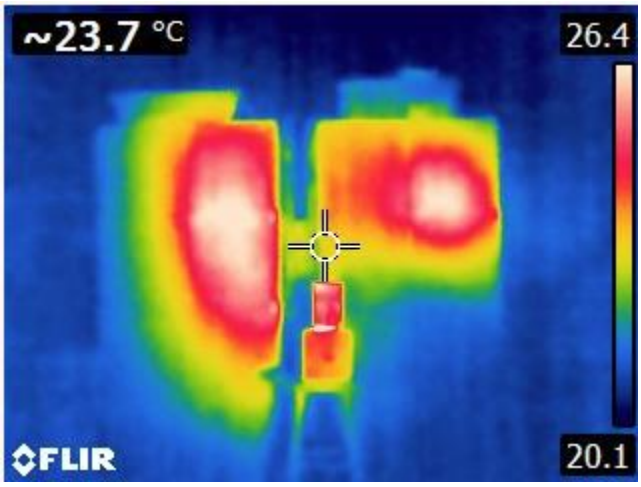

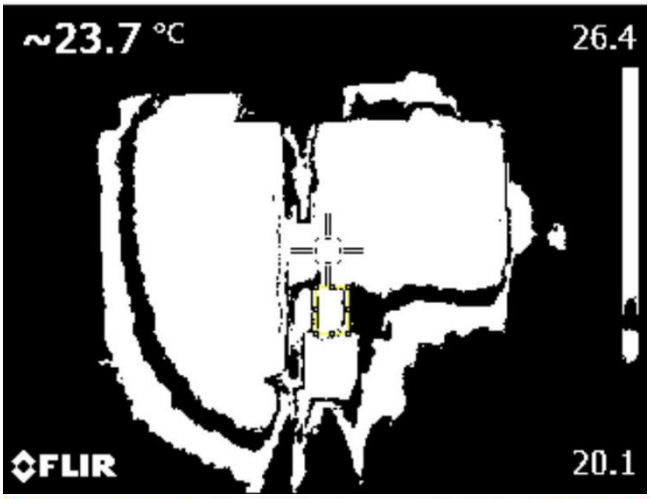
~23.7 °C
26.4
FLIR
20.1

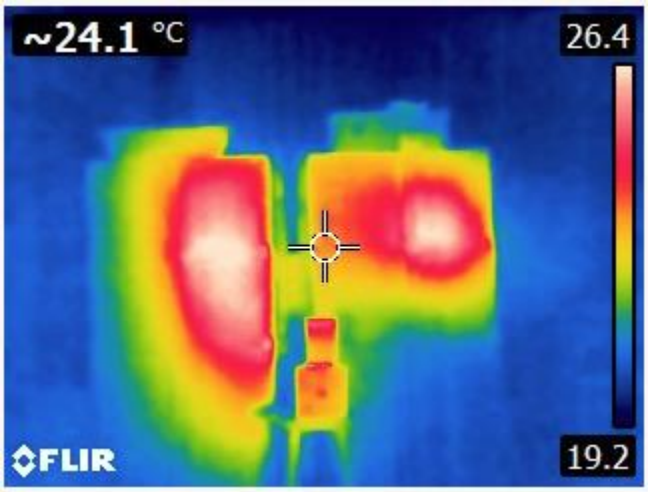
~24.1 °C
26.4
FLIR
19.2

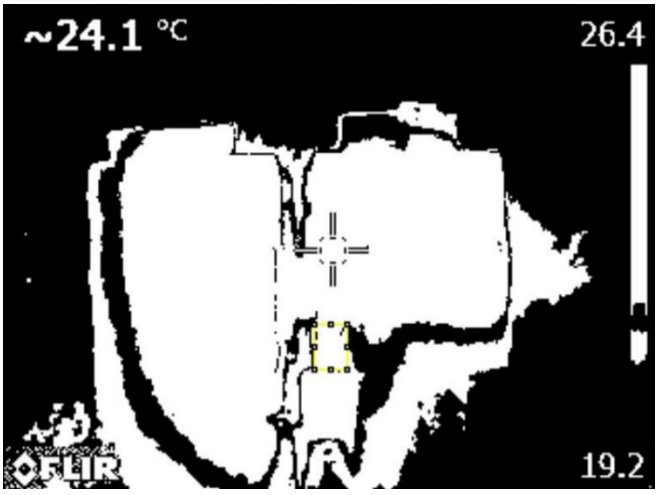
~24.1 °C
26.4
FLIR
19.2

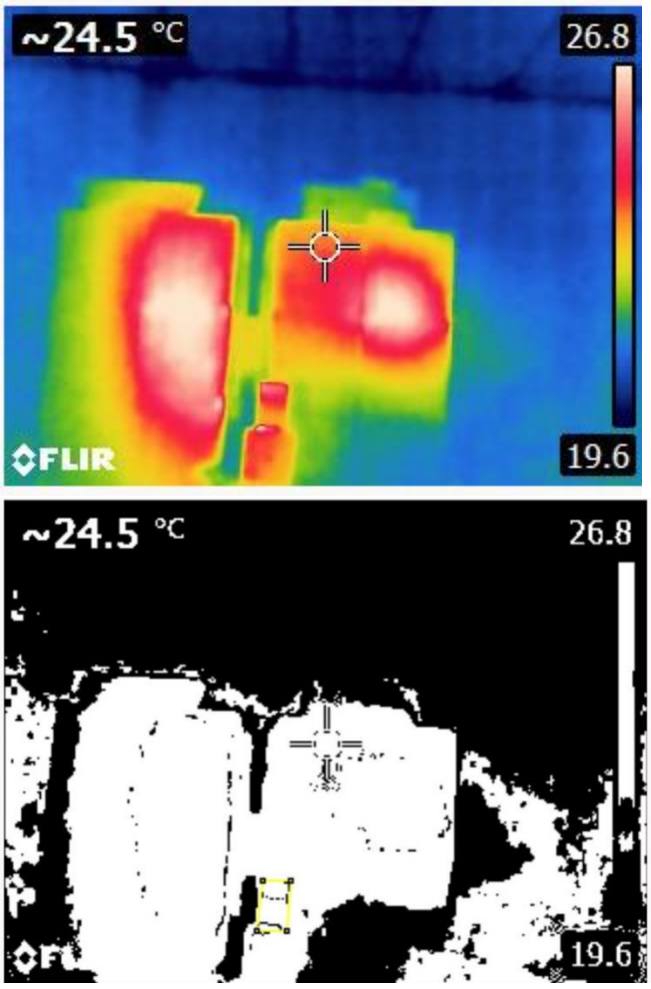

Sample 2

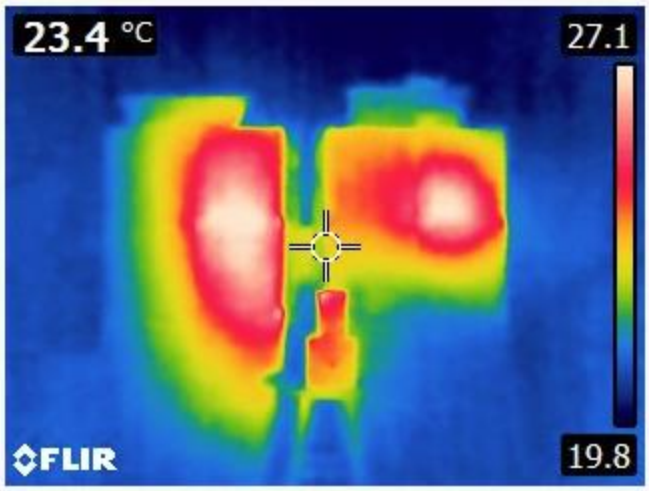
23.4 °C
27.1
FLIR
19.8

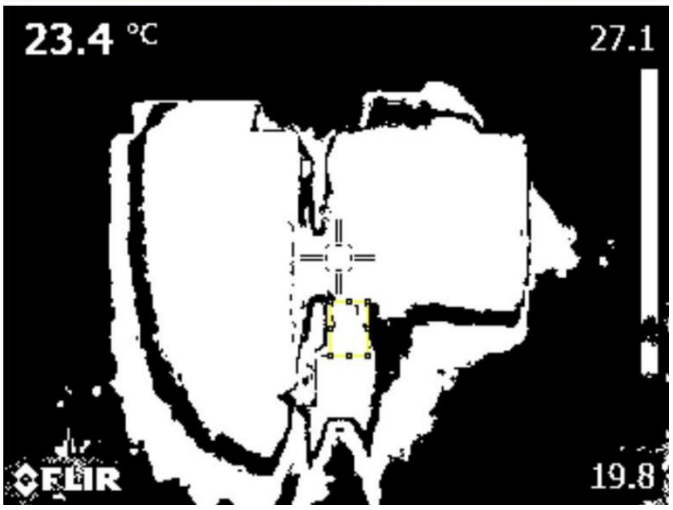
23.4 °C
27.1
FLIR
19.8

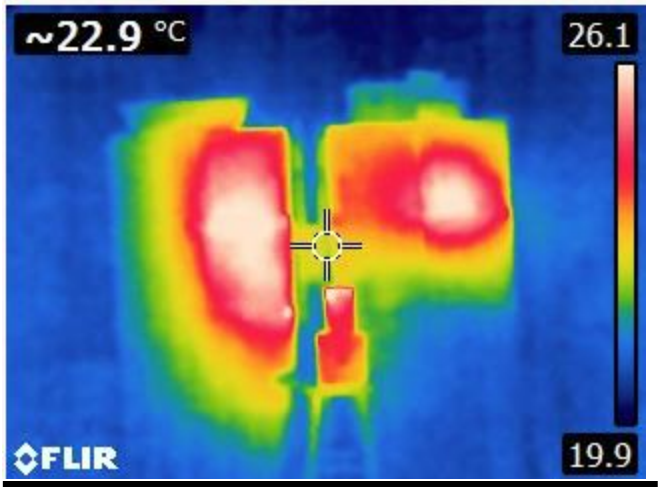
~22.9 °C
26.1
FLIR
19.9

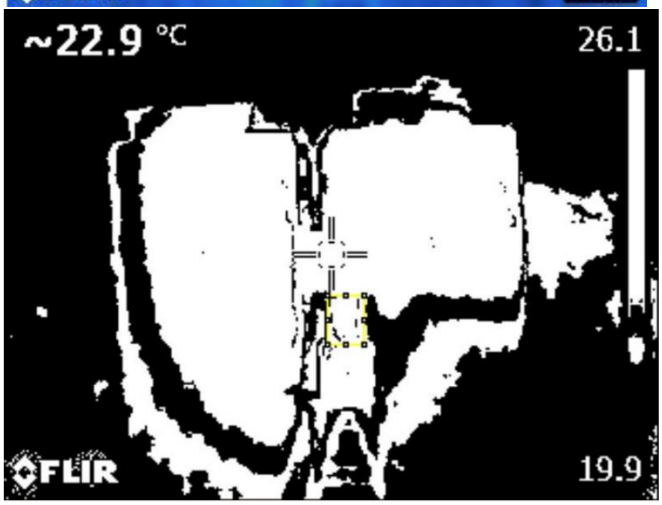
~22.9 °C
26.1
FLIR
19.9

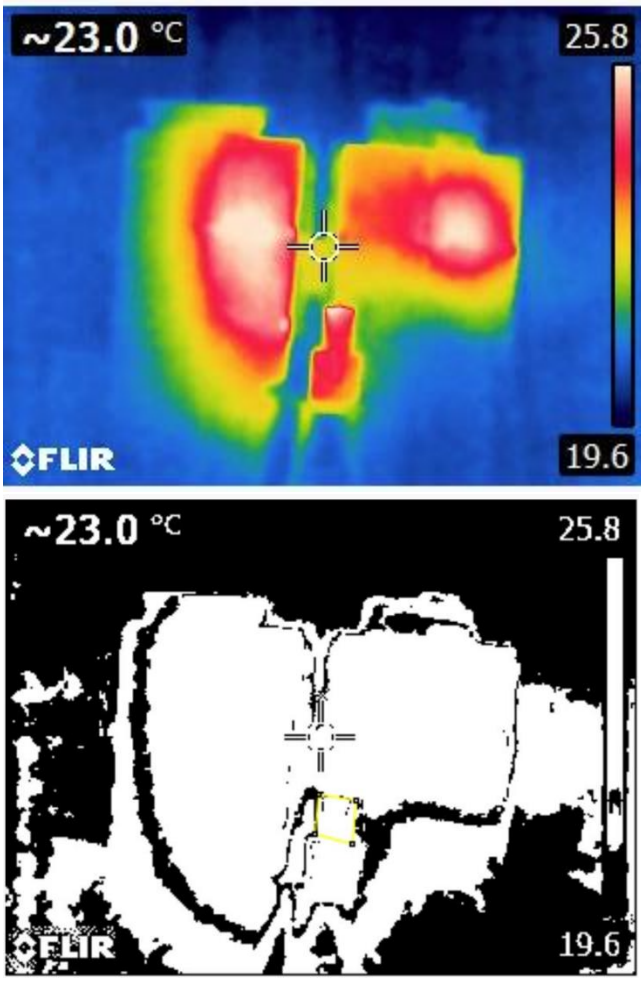

Sample 3

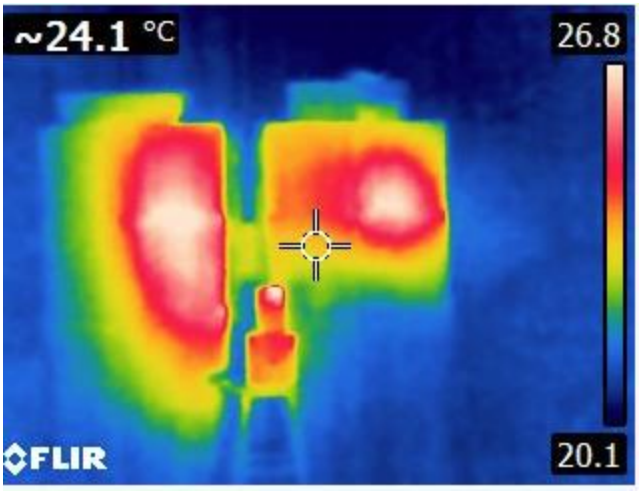
~24.1 °C
26.8
20.1
FLIR

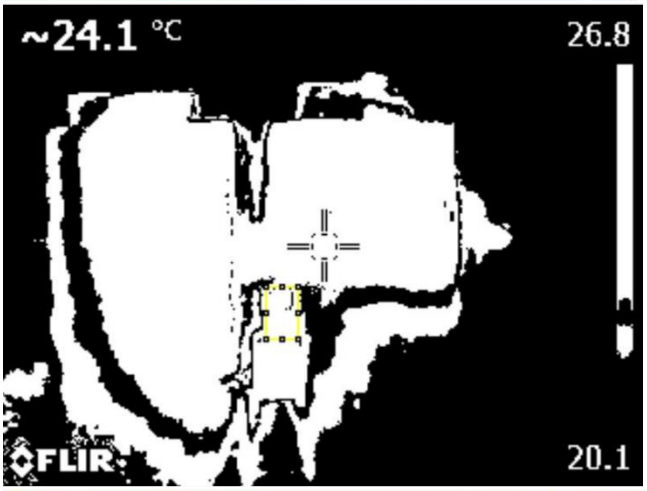
~24.1 °C
26.8
20.1
FLIR

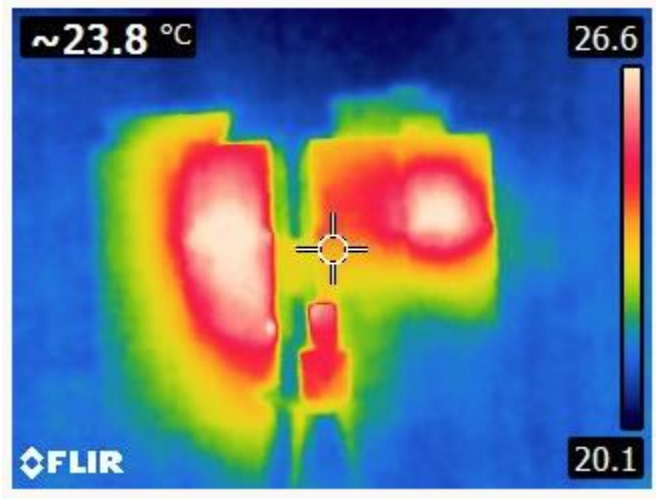
~23.8 °C
26.6
20.1
FLIR

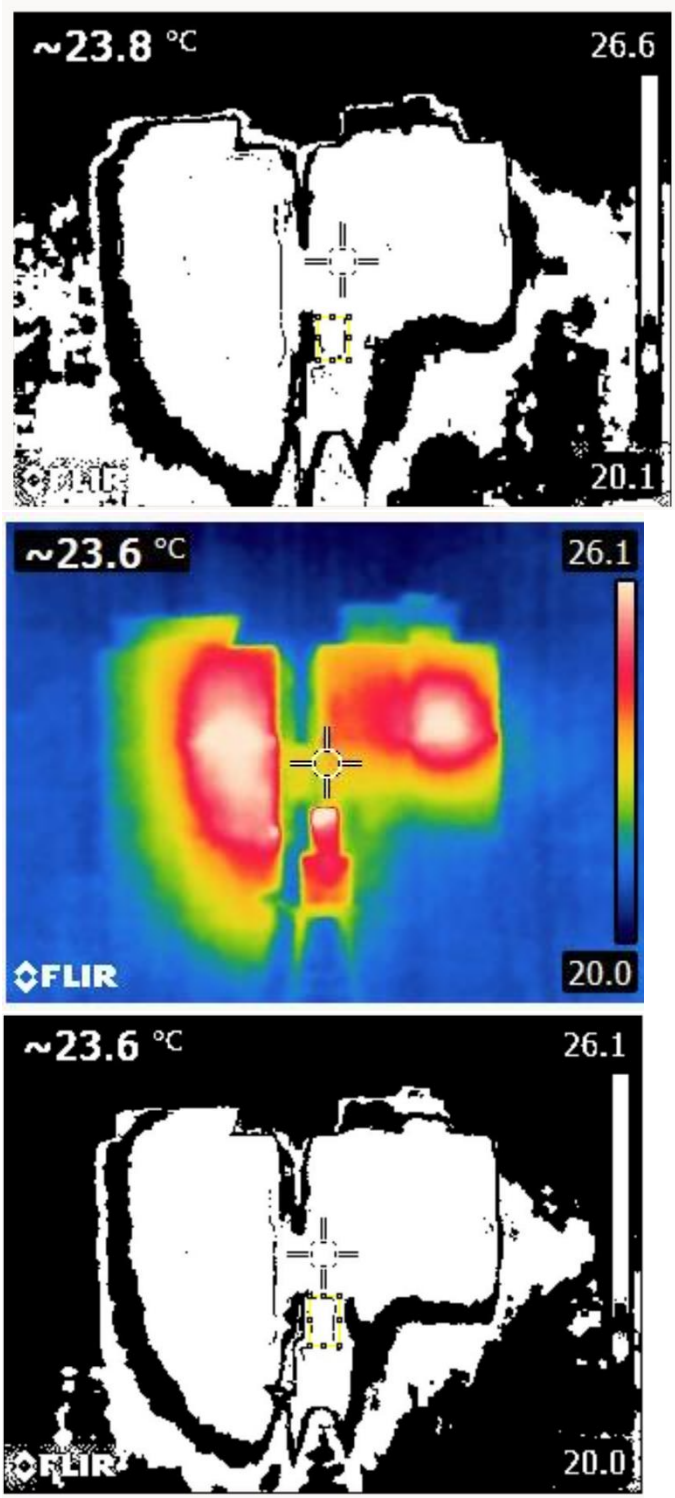

Composite samples thermographs and ImageJ images at 0.5 m.
Sample 1


max 22.2 °C
22.7
FLIR
18.6

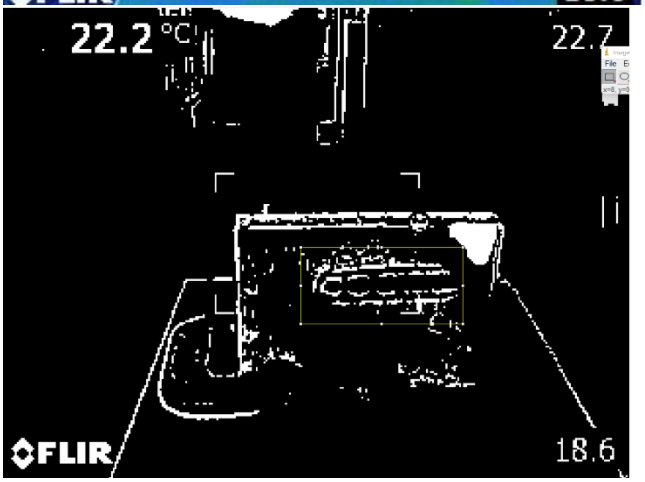
22.2 °C
22.7
FLIR
18.6

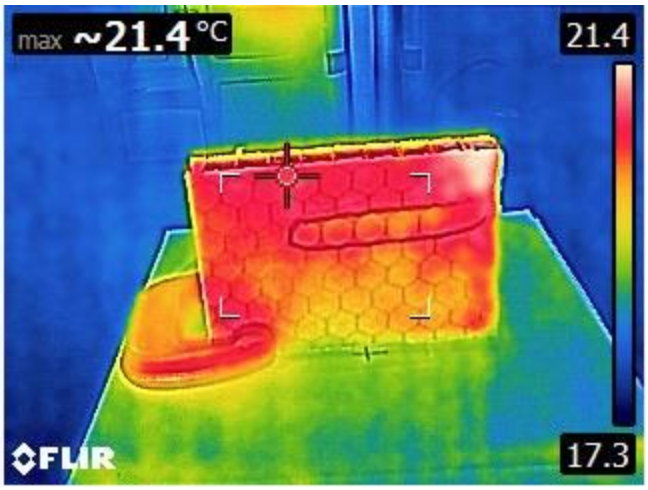
max ~21.4 °C
21.4
17.3
FLIR

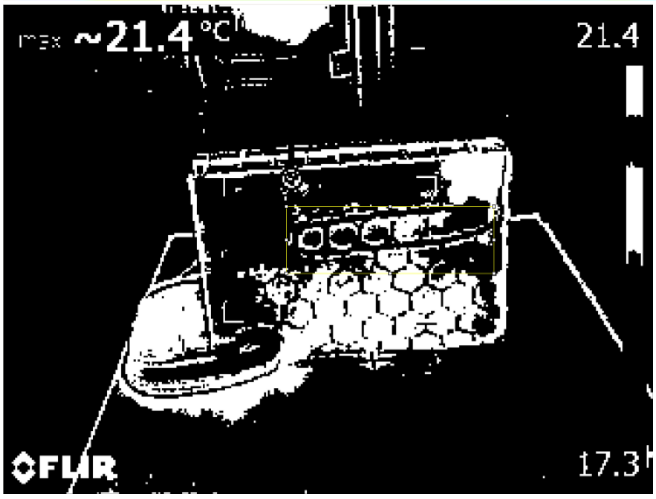
max ~21.4 °C
21.4
17.3
FLIR

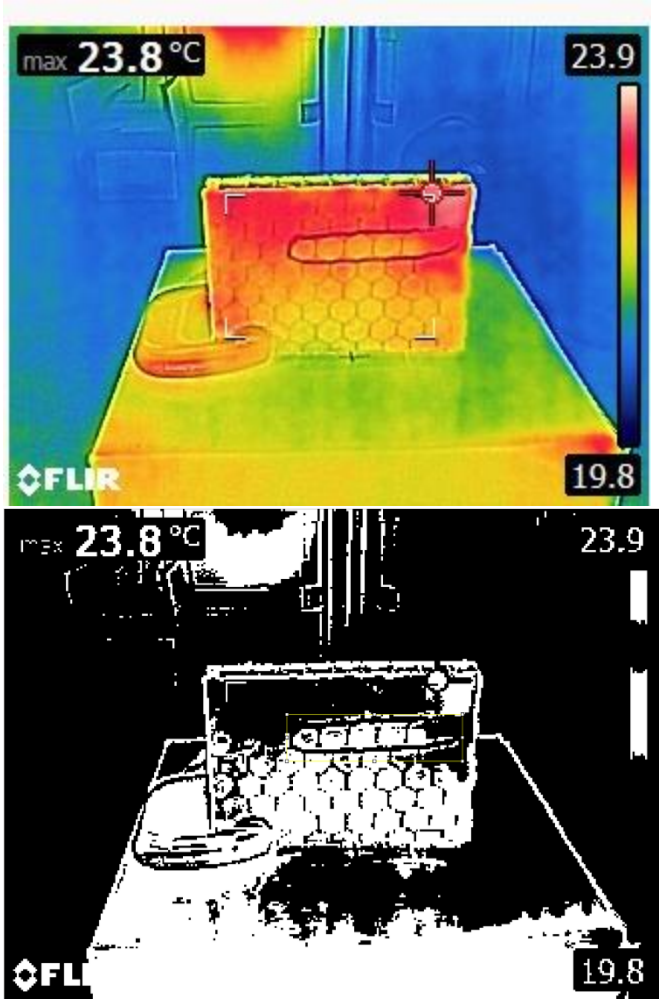

Sample 2

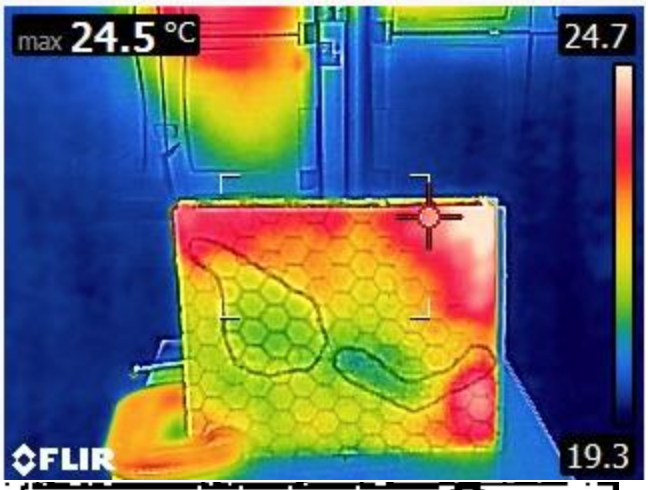
max 24.5 °C
24.7
19.3
FLIR

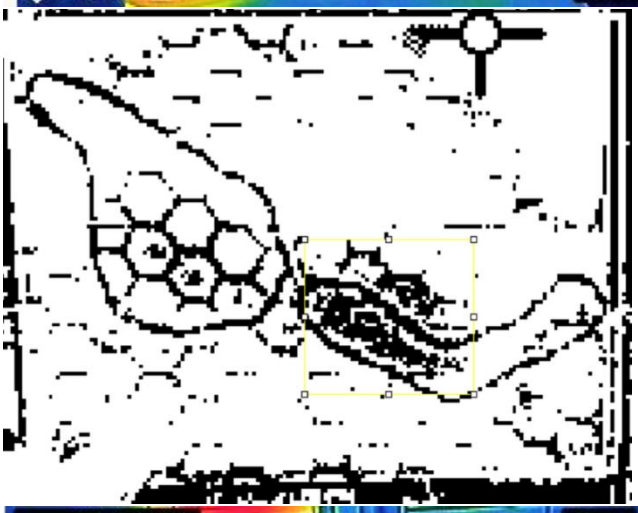

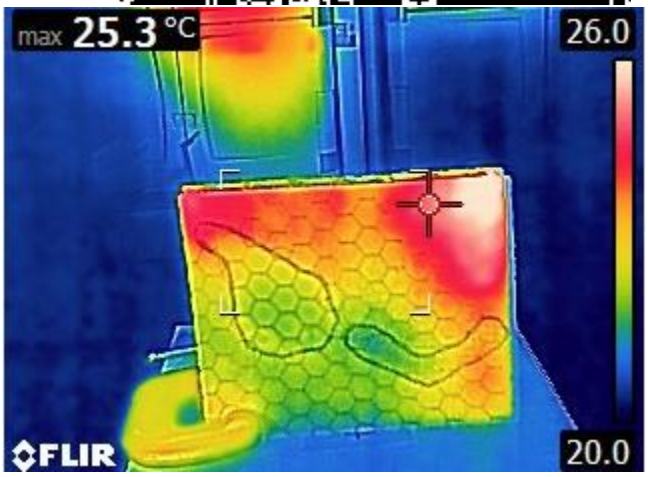
max 25.3 °C
26.0
20.0
FLIR

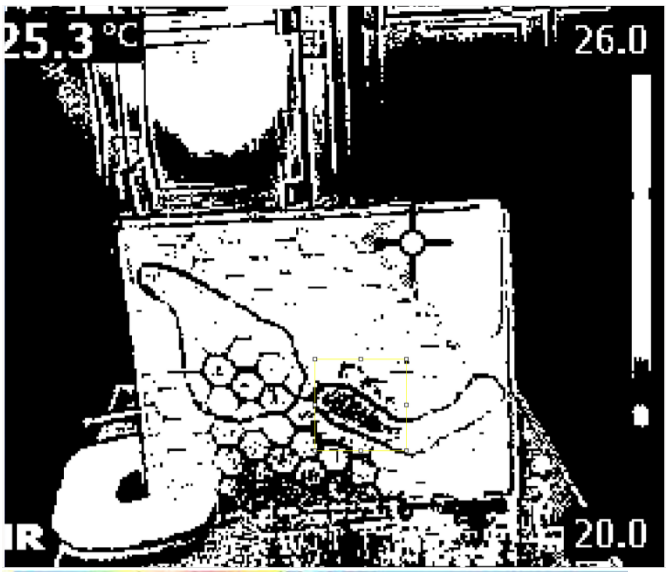
25.3 °C
26.0
20.0

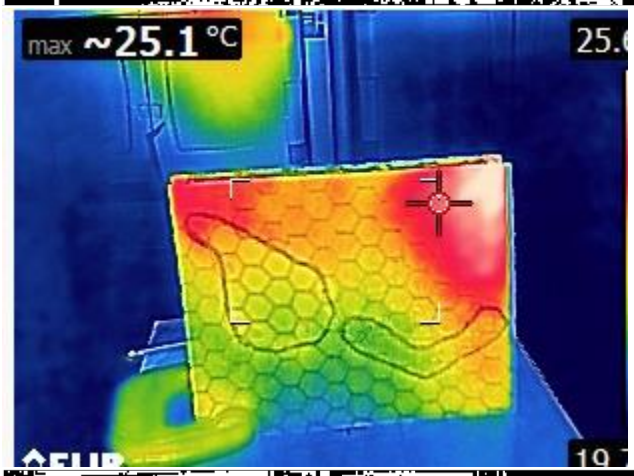
max ~25.1 °C

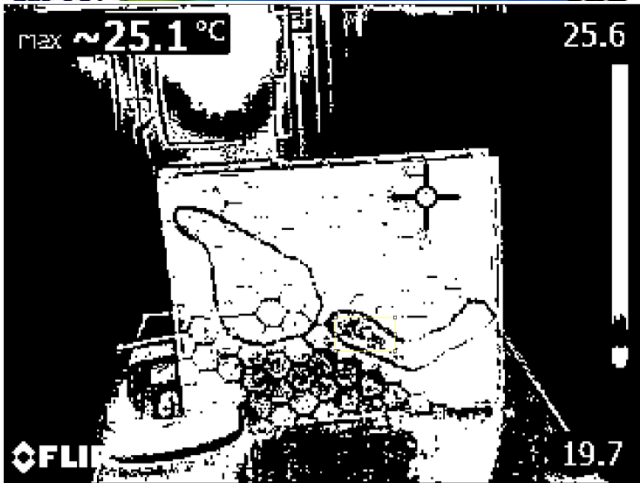
max ~25.1 °C
25.6
19.7

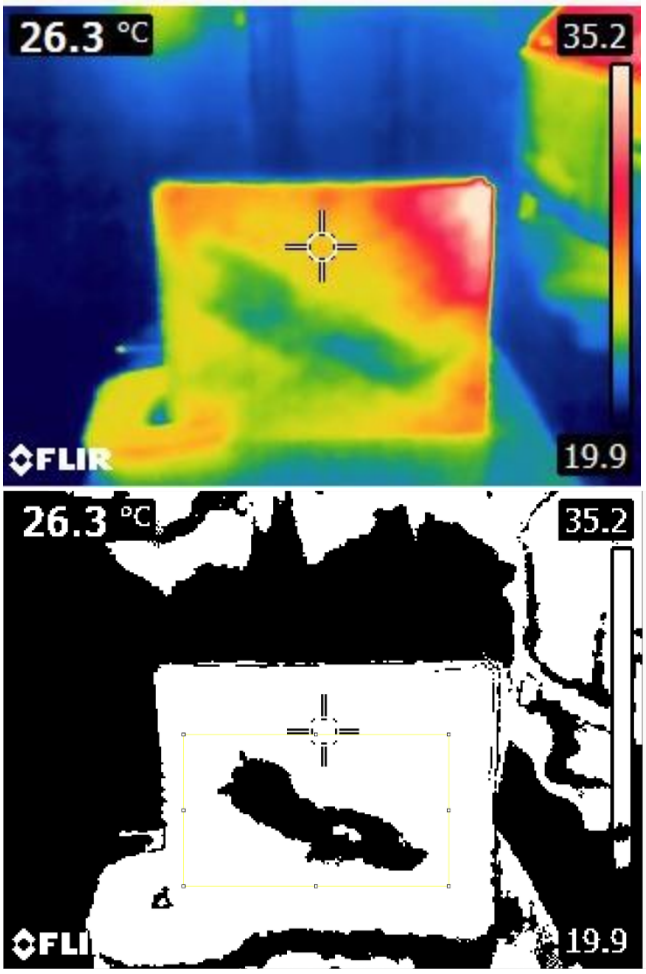

Sample 3

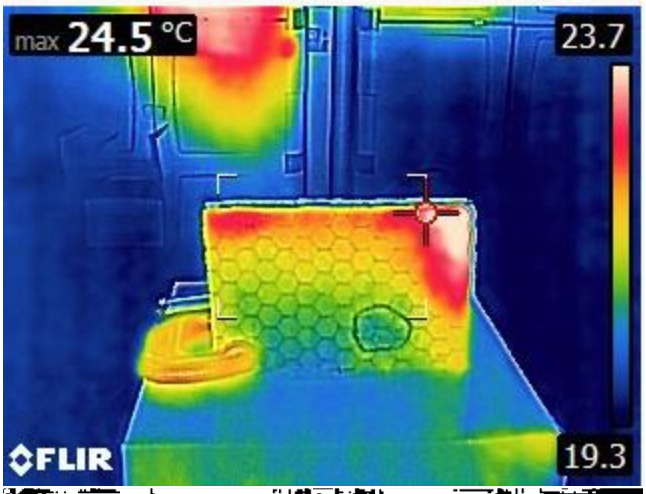
max 24.5 °C
23.7
FLIR
19.3


max 24.5 °C
23.7
FLIR
19.3


max 24.1 °C
24.7
FLIR
19.9

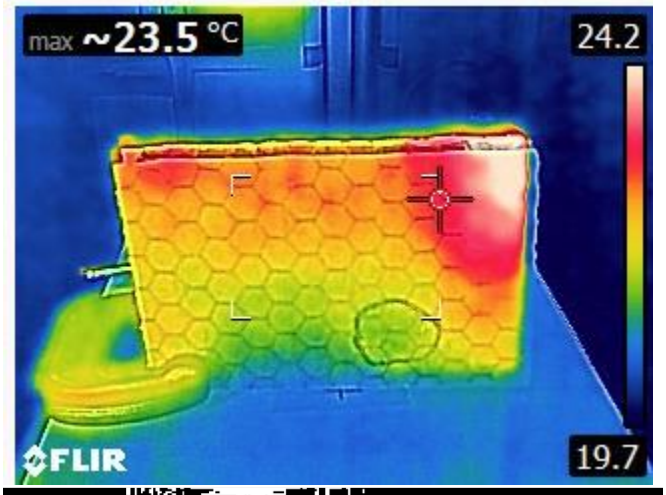

Composite samples thermographs and ImageJ images at 1.5 m.
Sample 1

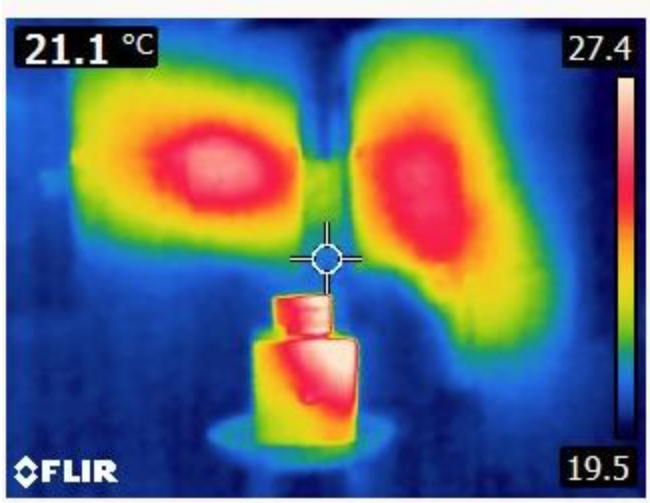
21.1 °C
27.4
FLIR
19.5

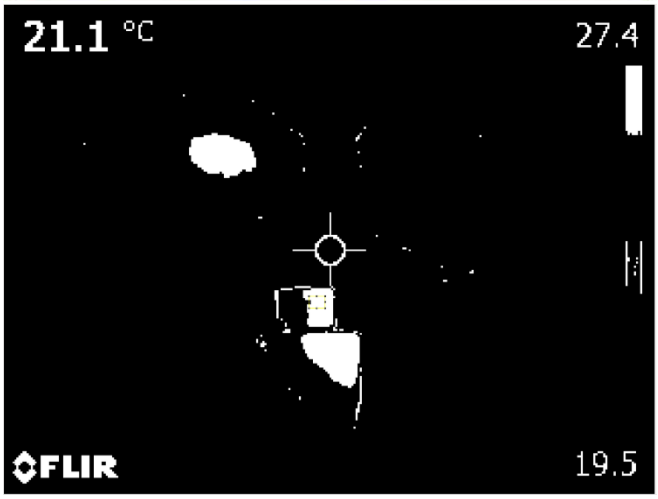
21.1 °C
27.4
FLIR
19.5

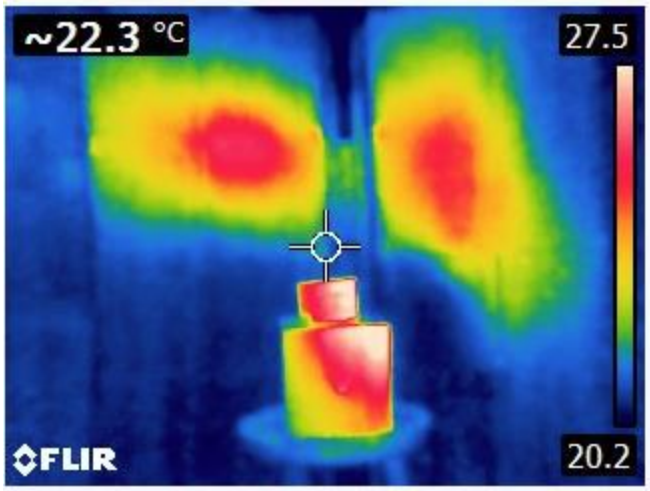
~22.3 °C
27.5
FLIR
20.2

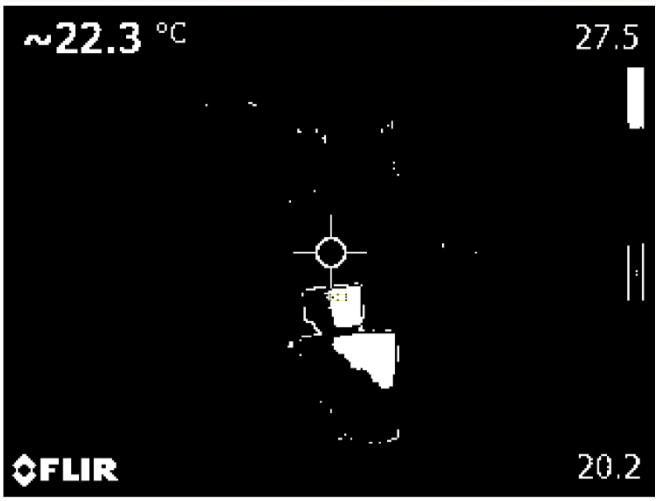
~22.3 °C
27.5
FLIR
20.2

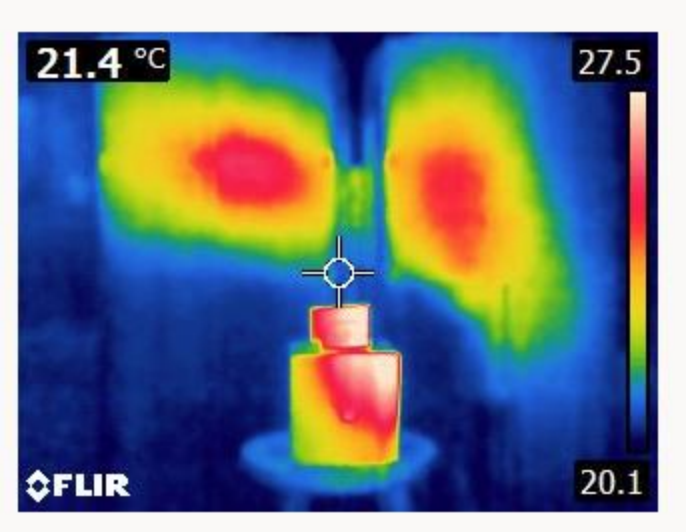

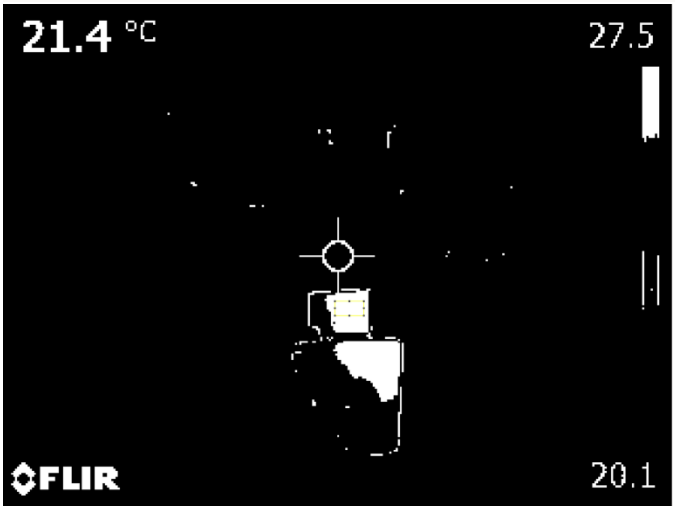

Sample 2

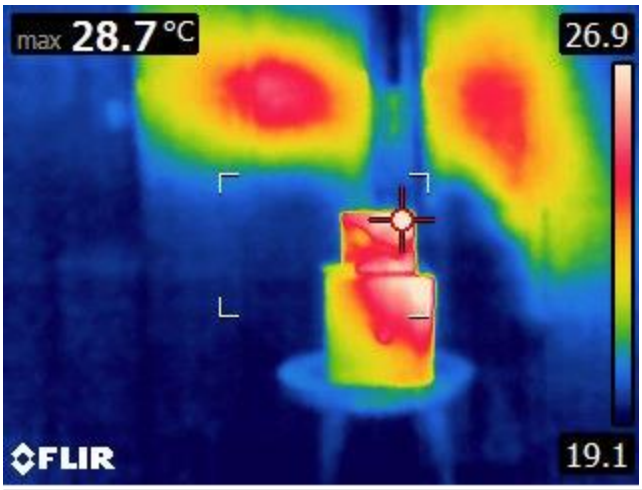
max 28.7 °C
26.9
FLIR
19.1


28.7 °C
26.9
FLIR
19.1

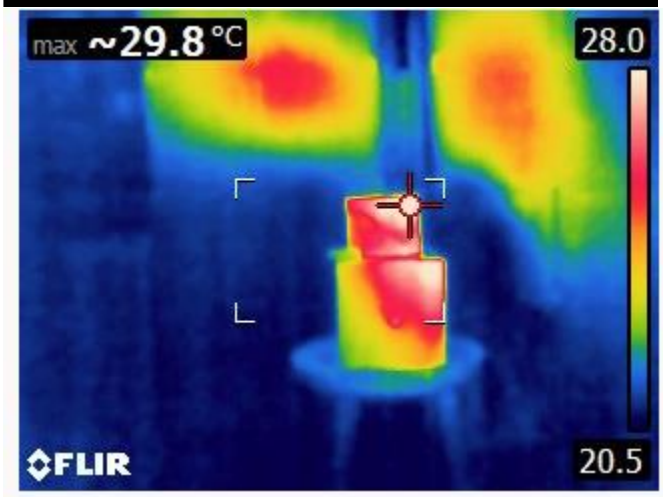
max ~29.8 °C
28.0
FLIR
20.5

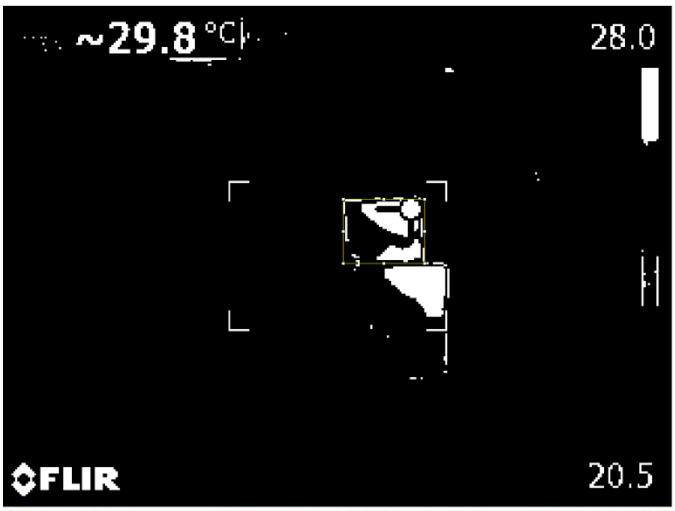

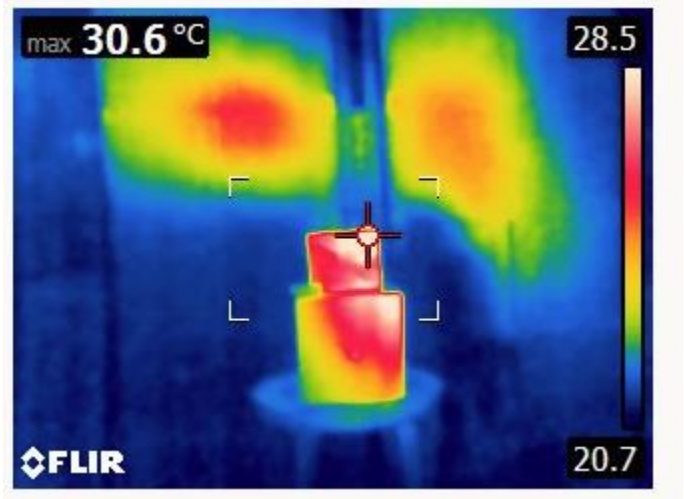

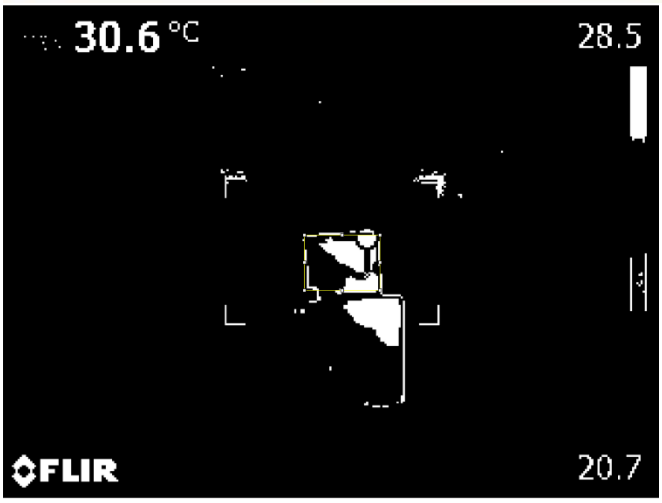

Sample 3

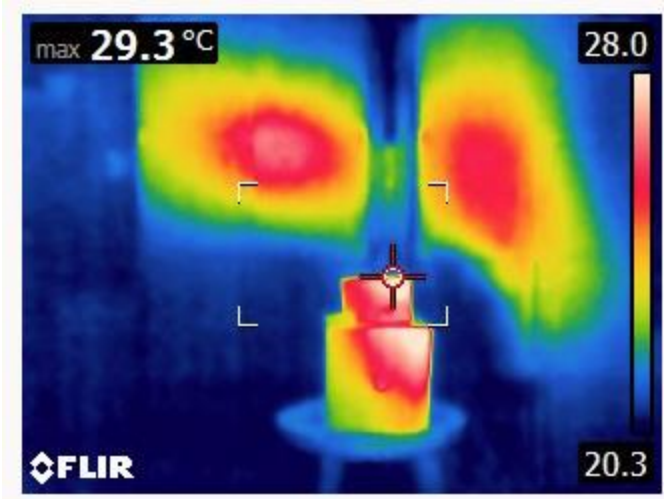
max 29.3 °C
28.0
FLIR
20.3

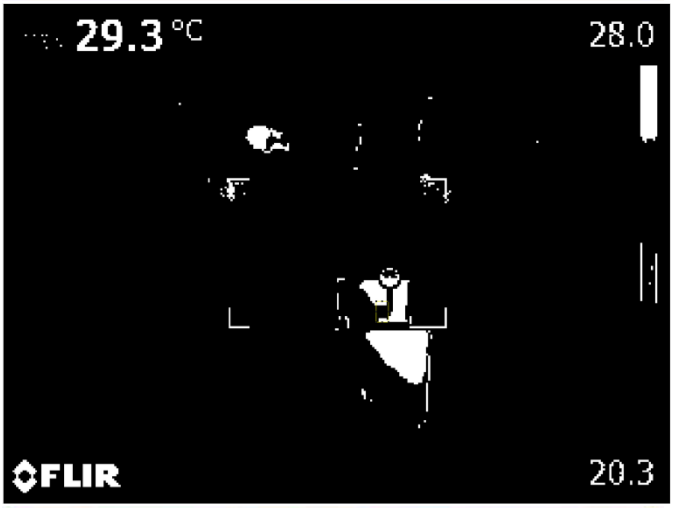
29.3 °C
28.0
FLIR
20.3

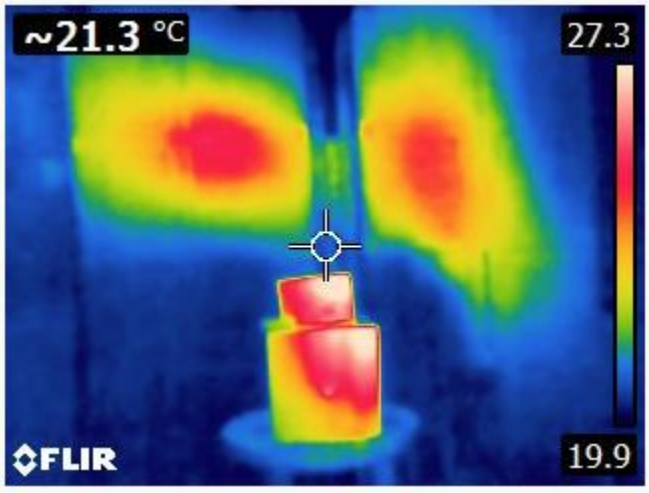
~21.3 °C
27.3
FLIR
19.9

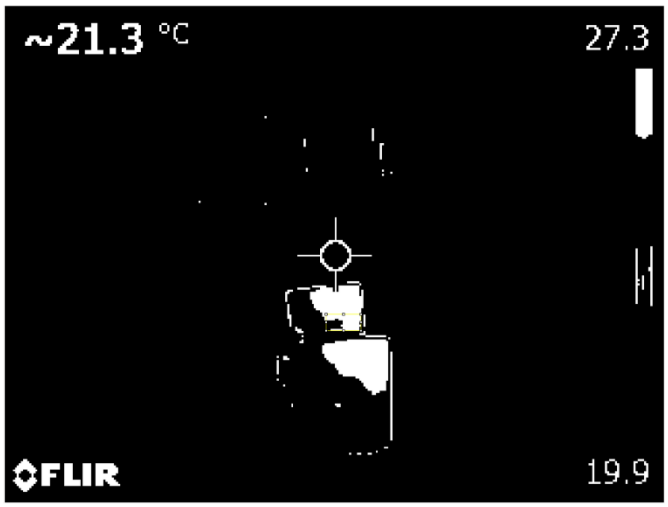

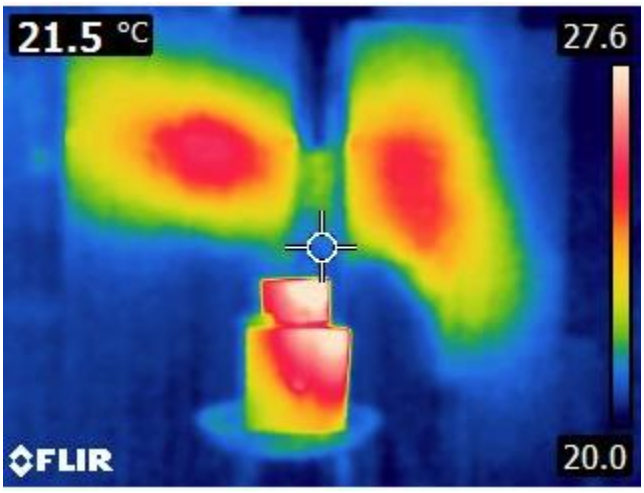

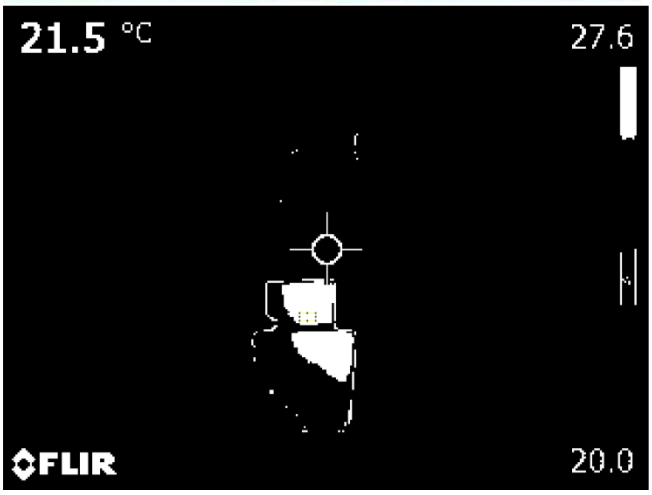

Composite samples thermographs and ImageJ images at 3.0 m.
Sample 1

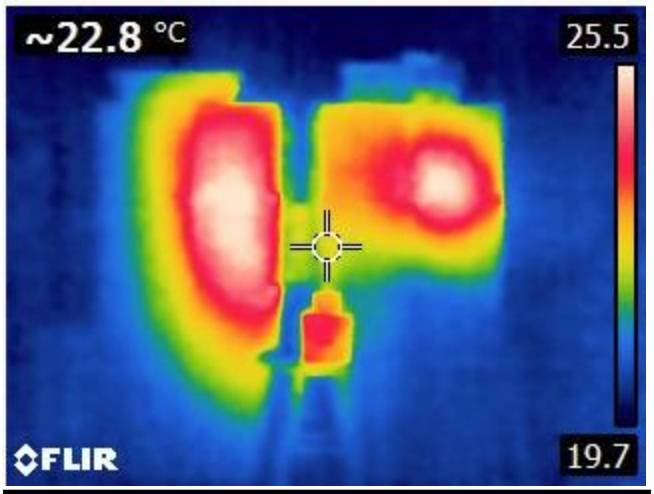
~22.8 °C
25.5
FLIR
19.7

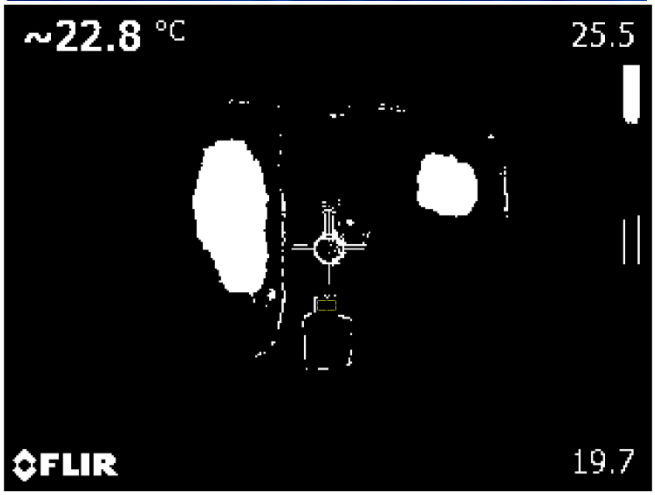
~22.8 °C
25.5
FLIR
19.7

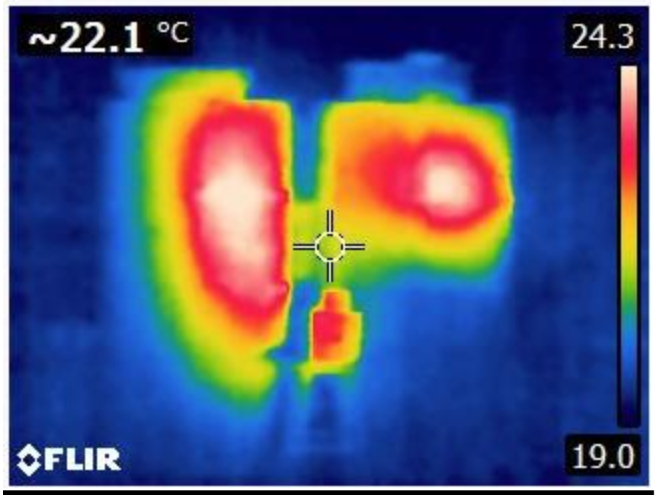
~22.1 °C
24.3
FLIR
19.0

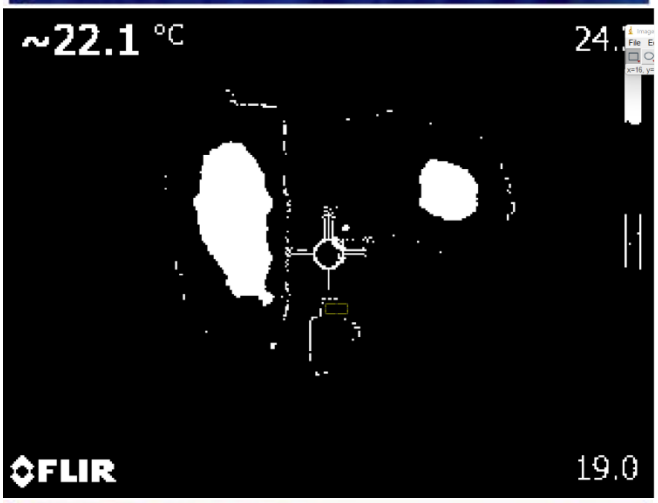
~22.1 °C
FLIR
19.0

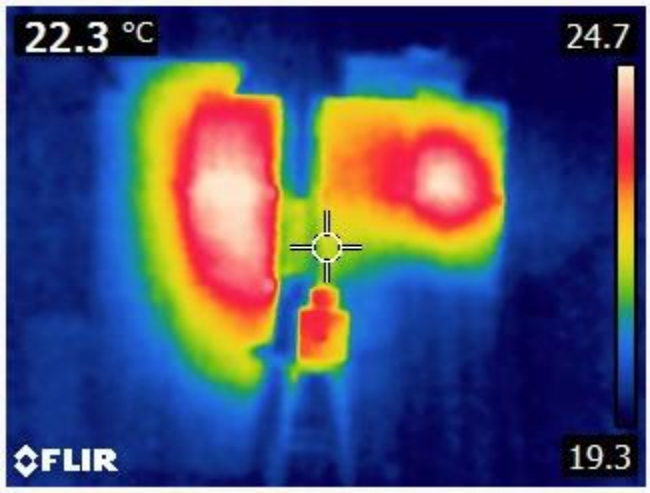
22.3 °C
24.7
FLIR
19.3

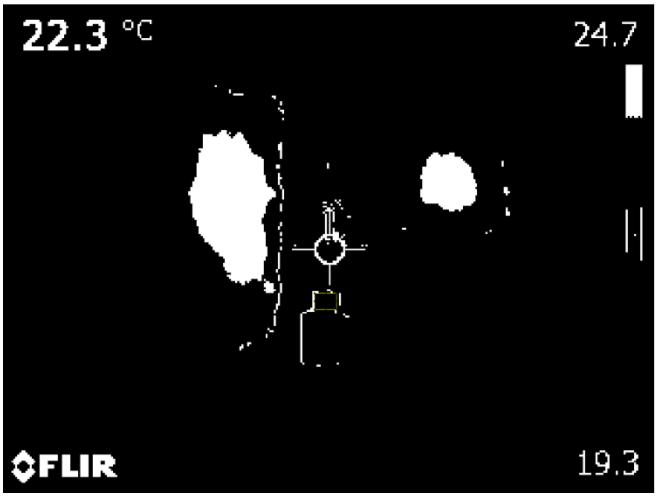

Sample 2

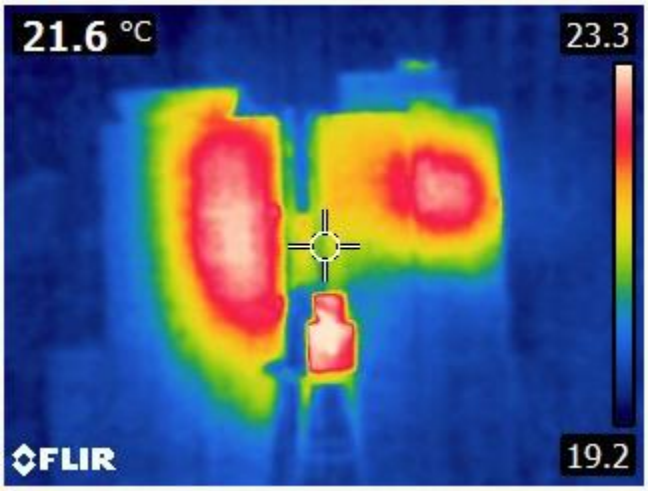

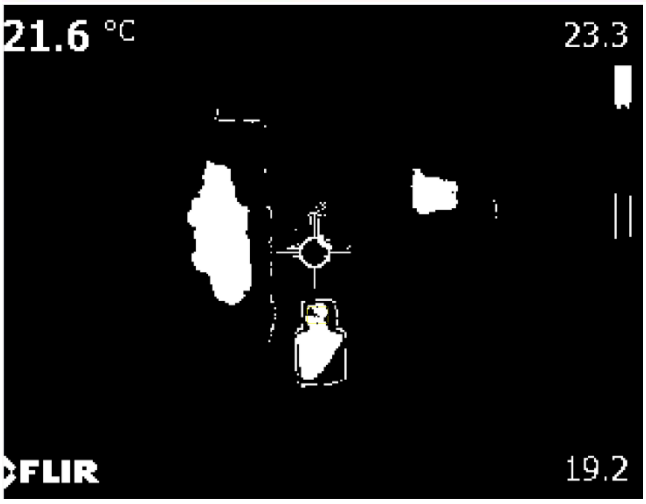

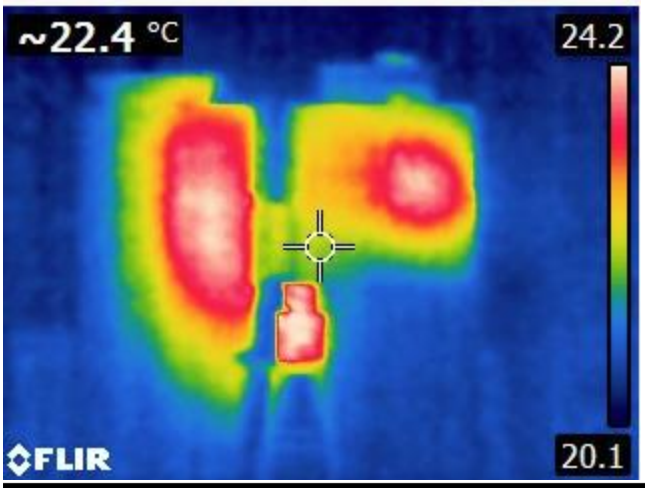
~22.4 °C
24.2
FLIR
20.1

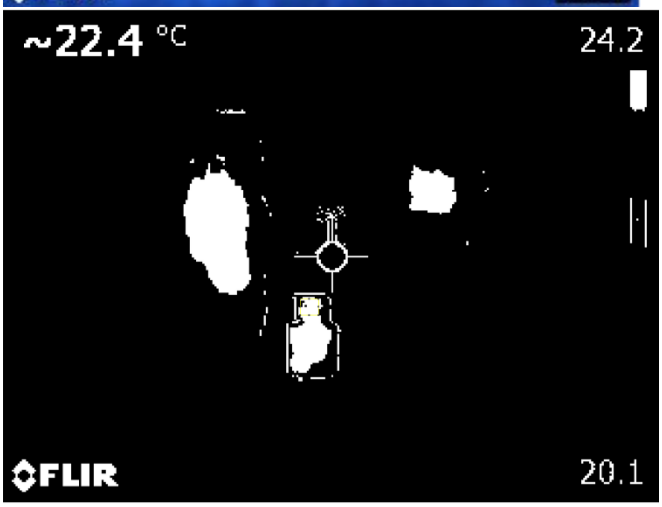
~22.4 °C
24.2
FLIR
20.1

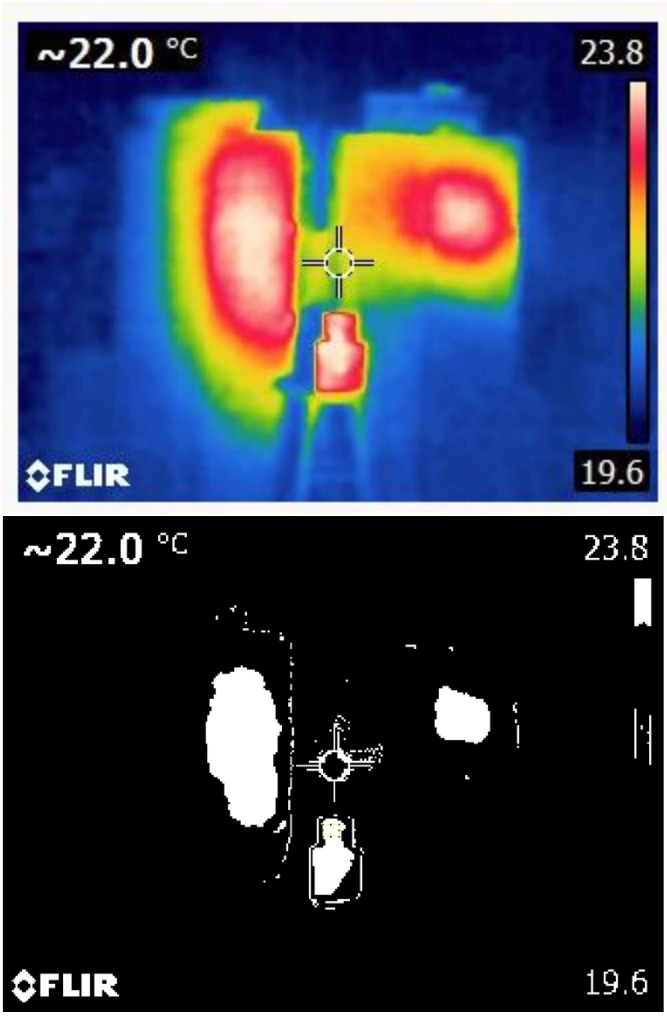

Sample 3

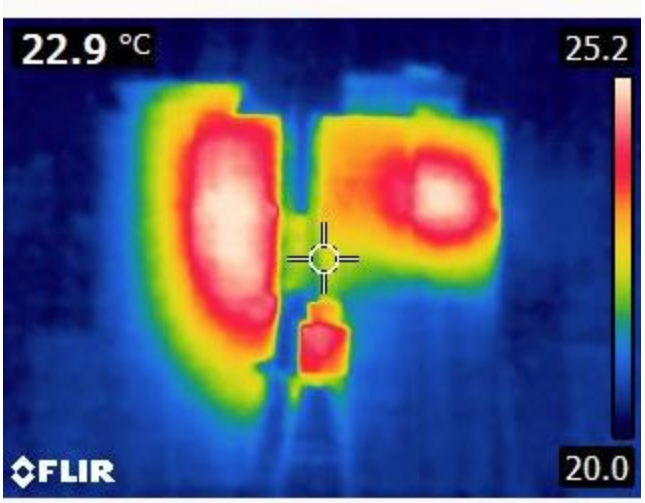
22.9 °C
25.2
FLIR
20.0

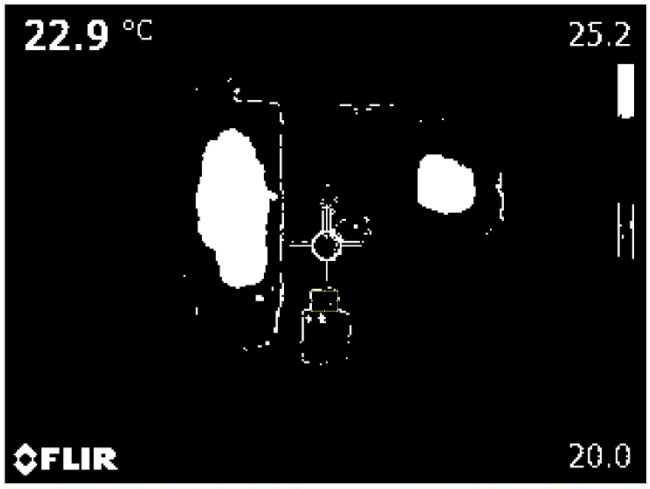
22.9 °C
25.2
FLIR
20.0

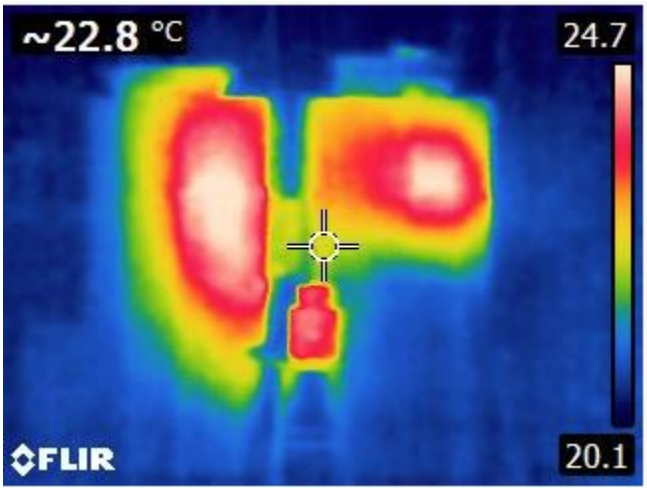
~22.8 °C
24.7
FLIR
20.1


~22.8 °C
24.7
FLIR
20.1

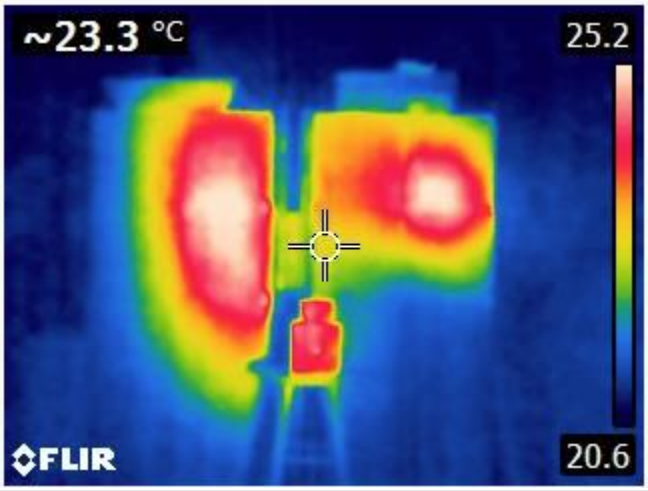
~23.3 °C
25.2
FLIR
20.6

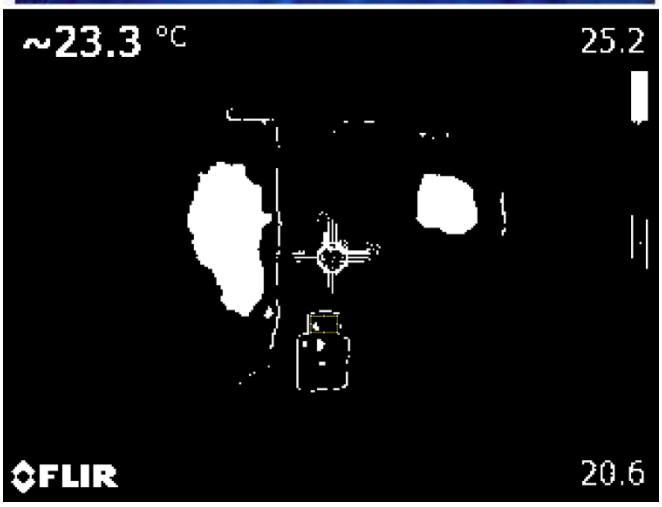
~23.3 °C
25.2
FLIR
20.6